The Ski2-family helicase Obelus regulates Crumbs alternative splicing and cell polarity

Athea Vichas,[1,2] Matthew T. Laurie,[1,2] and Jennifer A. Zallen[1,2]

[1]Developmental Biology Program and [2]Howard Hughes Medical Institute, Memorial Sloan Kettering Cancer Center, New York, NY 10065

Alternative splicing can have profound consequences for protein activity, but the functions of most alternative splicing regulators are not known. We show that Obelus, a conserved Ski2-family helicase, is required for cell polarity and adherens junction organization in the *Drosophila melanogaster* embryo. In *obelus* mutants, epithelial cells display an expanded apical domain, aggregation of adherens junctions at the cell membrane, and microtubule-dependent defects in centrosome positioning. Through whole-genome transcriptome analysis, we found that Obelus is required for the alternative splicing of a small number of transcripts in the early embryo, including the pre-mRNA that encodes the apical polarity protein Crumbs. In *obelus* mutants, inclusion of an alternative exon results in increased expression of a Crumbs isoform that contains an additional epidermal growth factor–like repeat in the extracellular domain. Overexpression of this alternative Crumbs isoform recapitulates the junctional aggregation and centrosome positioning defects of *obelus* mutants. These results indicate that regulation of Crumbs alternative splicing by the Obelus helicase modulates epithelial polarity during development.

Introduction

Alternative splicing increases protein diversity by generating multiple transcripts and protein isoforms from a single gene. Over 90% of intron-containing genes in humans are alternatively spliced, but the functional consequences of the vast majority of alternative splicing events are unknown (Wang et al., 2008; Brown et al., 2014). Alternative splicing plays an important role in a wide range of biological processes, including sex determination, axon guidance, neuronal arborization, immunity, and muscle differentiation, and defects in alternative splicing have been implicated in human disease (Faustino and Cooper, 2003; Tazi et al., 2009; Kalsotra and Cooper, 2011). Different isoforms of a single gene can perform distinct functions (Kelemen et al., 2013) and are often expressed in distinct temporal and spatial patterns (Graveley et al., 2011; Spencer et al., 2011; Brown et al., 2014). Splice-site selection in pre-mRNA transcripts is regulated by RNA-binding proteins that inhibit or promote the assembly of the spliceosome complex at particular splice sites (Fu and Ares, 2014). The molecular composition of the spliceosome itself can also vary between tissues, as spliceosomal proteins are expressed in different tissues and at different times during development, indicating that the spliceosome machinery is subject to extensive regulation (Park et al., 2004; Grosso et al., 2008; Celniker et al., 2009). Despite the pervasive presence and complexity of alternative splicing in multicellular organisms, the functions and molecular targets of most splicing regulators are currently unknown.

Epithelial cells are essential determinants of tissue structure, and defects in epithelial polarity and adhesion lead to developmental diseases and cancer. Cells in epithelia are connected by adherens junctions, which mediate cell interactions, maintain the structural integrity of the tissue, and enable dynamic tissue remodeling. The size, distribution, and dynamics of adherens junction complexes are regulated by several mechanisms, including interactions with the actin and microtubule cytoskeleton (Brieher and Yap, 2013), trafficking of junctional complexes to and from the plasma membrane (Wirtz-Peitz and Zallen, 2009), and spatial cues provided by the apical–basal polarity machinery (Harris and Tepass, 2010). Junctional proteins are distributed in a characteristic clustered fashion at the membrane, ranging from discrete puncta at nascent adherens junctions to a more continuous distribution at the mature zonula adherens (Tepass and Hartenstein, 1994; Adams et al., 1998; Cavey et al., 2008; McGill et al., 2009; Truong Quang et al., 2013). These clusters have been proposed to be important for the strength and dynamics of cell adhesion by increasing the avidity of weak intermolecular interactions and enabling rapid junctional remodeling during development (Yap et al., 2015). However, the mechanisms by which adherens junction organization is modulated by changes in the expression and activity of junctional regulators are not well understood.

Proteins involved in apical–basal polarity play an essential role in regulating adherens junction localization. Antagonis-

Correspondence to Jennifer A. Zallen: zallenj@mskcc.org

Abbreviations used in this paper: aPKC, atypical PKC; BAC, bacterial artificial chromosome; qRT-PCR, quantitative RT-PCR; UAS, upstream activator sequence.

The Rockefeller University Press $30.00
J. Cell Biol. Vol. 211 No. 5 1011–1024
www.jcb.org/cgi/doi/10.1083/jcb.201504083

tic interactions between apical and basolateral proteins direct the positioning of adherens junctions at the boundary between apical and basolateral domains (Bilder et al., 2003; Tanentzapf and Tepass, 2003; Blankenship et al., 2007). A transient expansion of the apical epithelial domain displaces adherens junctions basolaterally during tissue folding (Wang et al., 2012), and the apical domain is stably expanded in mature cells such as photoreceptors, which produce an elaborate apical light-sensing rhabdomere (Pellikka et al., 2002; Walther and Pichaud, 2010). The EGF repeat transmembrane protein Crumbs is an essential determinant of the apical domain and plays an important role in adherens junction organization in many tissues. Crumbs is required to maintain epithelial apical–basal polarity during development and to prevent light-induced degeneration of photoreceptor cells in the adult (Bulgakova and Knust, 2009; Tepass, 2012; Thompson et al., 2013). Crumbs and its associated proteins, Par-6, atypical PKC (aPKC), and Stardust/Pals1, act to exclude the junctional stabilizing protein Par-3 from the apical cortex, restricting Par-3 and adherens junctions to the adjacent junctional domain (Krahn et al., 2010; Morais de Sá et al., 2010; Walther and Pichaud, 2010). Overexpression of Crumbs leads to an expansion of the apical domain, raising the possibility that the level of Crumbs activity could provide a mechanism that modulates apical domain size (Wodarz et al., 1995; Grawe et al., 1996; Pellikka et al., 2002; Letizia et al., 2013). The *crumbs* pre-mRNA undergoes alternative splicing to produce three experimentally verified isoforms, each of which has a unique alteration in the extracellular domain (Brown et al., 2014). However, the factors that regulate the generation of different Crumbs isoforms, and how they influence epithelial polarity and junctional organization, are unknown.

Here, we report the identification of Obelus, a conserved Ski2-family DExD/H-box helicase isolated in a screen for *Drosophila melanogaster* mutants with defects in epithelial polarity and junctional organization. Embryos mutant for *obelus* display an expanded apical epithelial domain and aberrant aggregation of adherens junction proteins at the cell membrane, which are associated with a disruption of epithelial remodeling. Through whole-genome transcriptome analysis, we found that Obelus regulates the alternative splicing of the *crumbs* pre-mRNA. In *obelus* mutants, use of an alternative exon results in a switch in isoform expression of the *crumbs* pre-mRNA, resulting in increased expression of an isoform that contains an additional EGF-like repeat in the extracellular domain. Overexpression of this alternative Crumbs isoform is sufficient to recapitulate the centrosome mispositioning and junctional aggregation defects of *obelus* mutants. These results demonstrate that regulation of Crumbs alternative splicing by the Ski2-family helicase Obelus modulates cell polarity and adherens junction organization during development.

Results

obelus mutants have defects in adherens junction organization

To identify genes that regulate cell polarity and adhesion in epithelia, we screened for *Drosophila* mutants that have defects in body axis elongation, a conserved process of epithelial remodeling. We identified a spontaneous mutation in the *obelus* (*obe*) gene in the background of several pBac mutant lines (Schuldiner et al., 2008). The embryonic progeny of homozygous mutant *obe* females crossed to heterozygous males (referred to as *obe* mutants) displayed significantly reduced axis elongation compared with wild type (Fig. 1, C–E; and Fig. S1 A). The obe^{1} mutation failed to complement two deficiencies and a second mutation, obe^{2}, in the 88F6–88F7 interval on chromosome 3R (Fig. 1 D and Fig. S1 A). These mutations were all viable in trans but were male sterile and produced substantial maternal effect embryonic lethality (Fig. S1 A). These results indicate that obe^{1} and obe^{2} are alleles of a single gene that is required for epithelial remodeling and embryonic viability.

To determine whether these axis elongation defects are caused by a disruption of cell adhesion, we analyzed adherens junction localization in *obe* mutant embryos. During axis elongation in wild type, adherens junctions transition from discrete puncta to a more continuous distribution (Tepass and Hartenstein, 1994; Cavey et al., 2008; Truong Quang et al., 2013) and concentrate at dorsal and ventral cell borders in a planar polarized fashion (Zallen and Wieschaus, 2004; Blankenship et al., 2006). In *obe* mutants, the core adherens junction proteins E-cadherin and β-catenin and the junctional regulator Par-3 were enriched at dorsal and ventral cell borders as in wild type, indicating that planar polarity is correctly established (Fig. 1, A, B, and H–K). In contrast, adherens junctions showed an atypical clustering defect in a majority of *obe* mutant embryos. Par-3 was present in single, large aggregates at cell interfaces (Fig. 1, A and B). These aggregates colocalized with E-cadherin and β-catenin and failed to resolve into a continuous distribution during axis elongation (Fig. 1, H–K). Similar defects were observed in multiple *obe* alleles (Fig. S1, B–D). Junctional aggregates in *obe* mutants were more pronounced during axis elongation (stages 6–8), and a more uniform junctional distribution was restored at later stages (Fig. S1, E and F). These results demonstrate that Obelus is required for adherens junction localization and body axis elongation.

Obelus is required for centrosome positioning in epithelial cells

We observed several phenotypes in *obe* mutants that are commonly associated with defects in microtubule or centrosomal organization, including uncoordinated movement in adults, male sterility, and immobile flagella in sperm motility assays (unpublished data). We therefore tested whether *obe* mutants had defects in centrosome localization. Epithelial formation in the *Drosophila* embryo coincides with the reorganization of microtubules from a radial array focused at centrosomes to a noncentrosomal cortical array aligned with the apical–basal axis (Warn and Warn, 1986). In stage 5, centrosomes are located near the apical cortex in close proximity to cortical microtubules, consistent with their role as microtubule-organizing centers (Fig. 2 A). In stage 6, centrosomes dissociate from cortical microtubules and move away from the cortex to occupy a more basal and centrally located position within the cell (Fig. 2, C and G–I). In contrast, although a majority of wild-type centrosomes had moved away from the apical cortex by stage 7 (80 ± 5%), a smaller fraction of centrosomes had successfully moved away from the apical cortex by this stage in *obe* mutants (17 ± 3%; $P < 0.0001$; Fig. 2, B and D–F). Most centrosomes failed to dissociate from microtubules in *obe* mutants and instead remained in close proximity to adherens junctions throughout axis elongation in stages 6 and 7 (Fig. 2, J–L). Mispositioned centrosomes were often associated with adherens junction aggregates, such that two centrosomes flanked a single

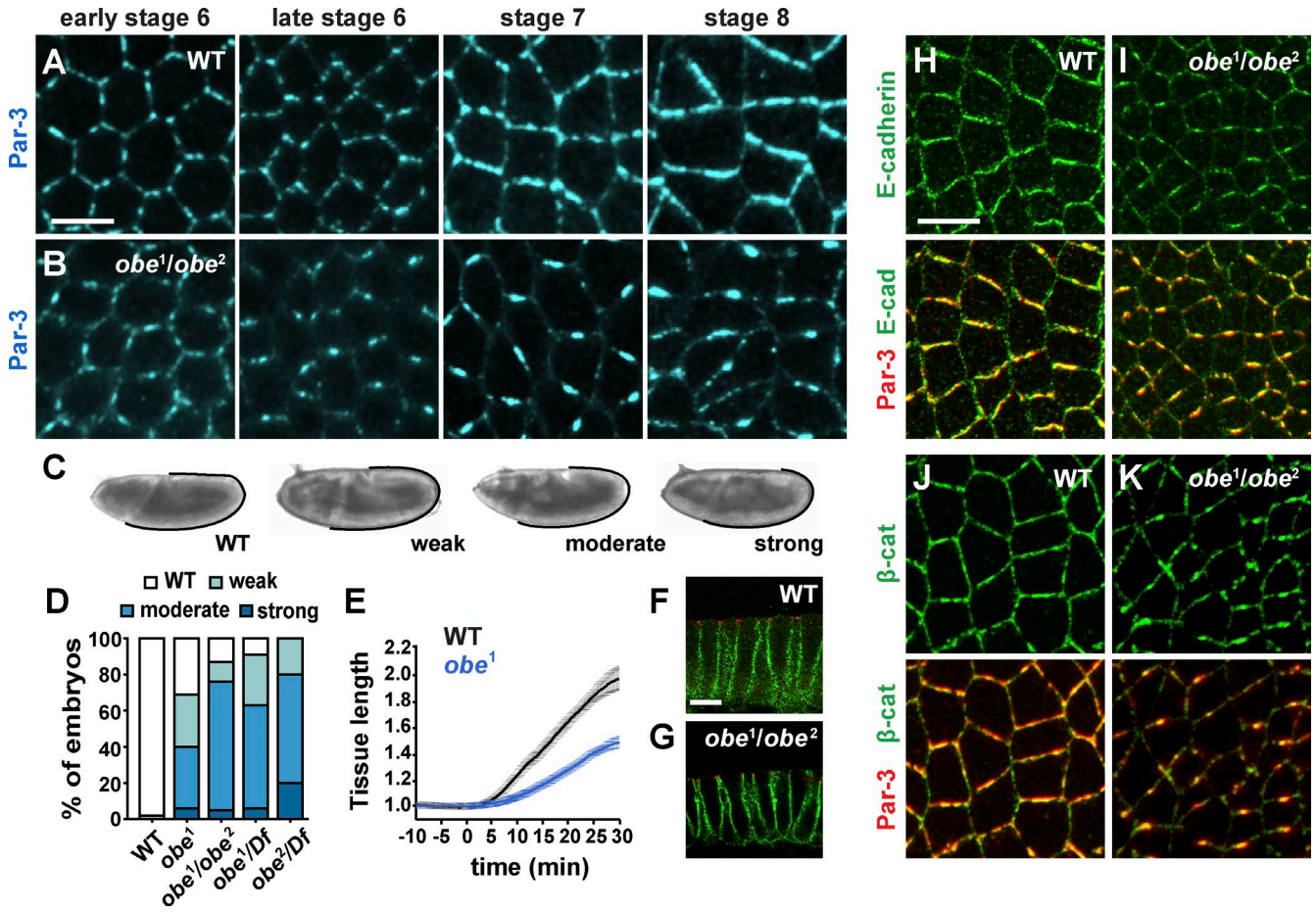

Figure 1. **Obelus regulates the localization of adherens junction proteins.** (A and B) Localization of Par-3 in wild-type (WT) embryos and *obe*^{1}/*obe*^{2} mutants. Par-3 aggregates were observed in 71% of *obe*^{1} (n = 24), 92% of *obe*^{1}/*obe*^{2} (n = 26), and 100% of *obe*^{2}/*Df* embryos (n = 12) at stage 7, compared with 4% in wild type (n = 23). (C) Stills from bright-field videos of wild-type and *obe*^{1} mutants 30 min after the onset of elongation (germband, black line) with weak (50% egg length), moderate (30–40% egg length), or strong (<20% egg length) defects. (D) Axis elongation in bright-field videos of wild-type and *obe* mutant embryos (n = 62–93 embryos per genotype). (E) Axis elongation based on automated cell tracking in embryos expressing Resille :GFP. Elongation was significantly reduced in moderate *obe*^{1} mutants (n = 4 wild type and 3 *obe*^{1} videos; $P < 0.006$ by unpaired t test [t = 30 min value as the test statistic]). Tissue length along the anterior–posterior axis was normalized to the length at t = 0. The mean ± SEM between embryos is shown. (F and G) β-Catenin (red) and neurotactin (green) in stage 7 wild-type and *obe*^{1}/*obe*^{2} mutant embryos. (H–K) Par-3, E-cadherin, and β-catenin in stage 7 wild-type and *obe*^{1}/*obe*^{2} mutant embryos. The *obe*^{1} embryos were the progeny of *obe*^{1}/*obe*^{1} females crossed to *obe*^{1}/+ males. The *obe*^{1}/*obe*^{2} and *obe*^{2}/*Df* embryos were the progeny of *obe*^{1}/*obe*^{2} and *obe*^{2}/*Df(3R)Exel6174* females, respectively, crossed to *obe*^{2}/+ males. (A–C and H–K) Anterior left, dorsal up. (F and G) Cross sections, apical up. Bars, 10 µm. See also Fig. S1.

aggregate (an arrangement that resembles the division symbol, also known as an obelus). These results show that *obe* mutants have defects in centrosome positioning and adherens junction localization, indicating that Obelus is required for multiple aspects of cell polarity.

The cell polarity defects in *obelus* mutants require dynamic microtubules

Centrosome positioning and adherens junction organization both require the microtubule cytoskeleton (Harris and Peifer, 2007; Siegrist and Doe, 2007). We therefore hypothesized that the defects in *obe* mutants could result in part from disrupted microtubule localization or activity. To test this possibility, we treated permeabilized *obe* mutant embryos with a low concentration of the microtubule-depolymerizing drug nocodazole, which inhibits microtubule polymerization without substantially disrupting overall microtubule levels (Liao et al., 1995). A brief (7 min) incubation of wild-type embryos in nocodazole caused a slight reduction in the level of cytosolic microtubules associated with centrosomes (Fig. 3, A and B). This treatment did not affect centrosome positioning in wild type, but did cause a reduction of cortical Par-3, consistent with the role of dynamic microtubules in cell adhesion. Notably, nocodazole treatment fully rescued the centrosome positioning defects in *obe* mutants (Fig. 3, C–E). In addition, nocodazole treatment completely suppressed the Par-3 aggregation defects in *obe* mutants, eliminating Par-3 puncta and restoring a more uniform distribution of Par-3 at the dorsal and ventral cell borders, similar to wild type (Fig. 3, D and E). These results demonstrate that the adherens junction aggregation and centrosome positioning defects in *obe* mutants are microtubule dependent.

The aberrant association between adherens junctions and centrosomes in *obe* mutants and the restoration of wild-type junctional localization and centrosome positioning by nocodazole treatment suggest that these defects may be caused by aberrant microtubule-nucleating activity at centrosomes. To test this possibility, we analyzed the localization of γ-tubulin, which is required for the microtubule-nucleating activity of centrosomes

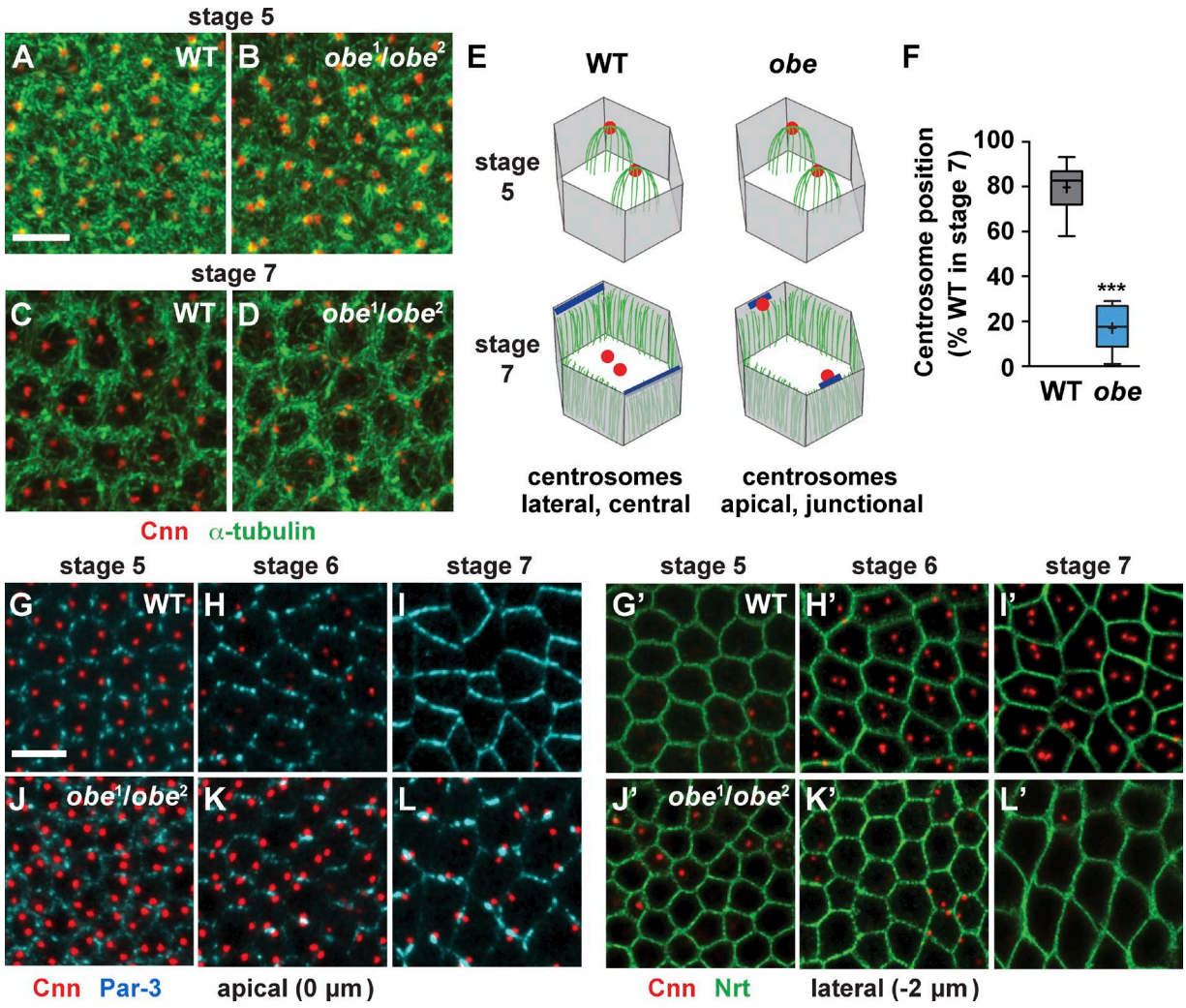

Figure 2. **Centrosomes are mispositioned along the apical–basal axis in *obelus* mutants.** (A–D) Localization of microtubules (α-tubulin) and centrosomes (Cnn) in wild-type (WT) and obe^1/obe^2 mutant embryos. A single z plane at the level of the centrosomes is shown. (E) Centrosomes fail to dissociate from microtubules in *obe* mutants and remain embedded in cortical microtubule arrays. (F) The percentage of centrosomes that correctly relocalized laterally in stage 7 was strongly reduced in obe^1/obe^2 mutants. Boxes, 25–75th percentile. Whiskers, 5–95th percentile. Horizontal line, median. +, mean. Plot shows the distribution of mean values across embryos (24–43 cells analyzed per embryo in 6–10 embryos per genotype). ***, $P < 0.0001$ by unpaired *t* test. (G–L) Centrosomes in wild-type and obe^1/obe^2 mutant embryos shown in two planes at the level of the apical adherens junctions (Par-3) and 2 µm below the adherens junctions (neurotactin [Nrt]). (G–I) Wild-type centrosomes move basally and toward the center of the cell in stage 6. (J–L) In *obe* mutants, centrosomes fail to move basally and remain associated with adherens junctions. The obe^1/obe^2 mutant embryos were the progeny of obe^1/obe^2 females crossed to $obe^2/+$ males. Anterior left, dorsal up. Bars, 10 µm.

(Stearns and Kirschner, 1994). In wild-type embryos, γ-tubulin is rapidly down-regulated at centrosomes in stage 6, indicating that centrosomes lose their microtubule-nucleating activity as they move away from the cortex (Fig. S2, A and C). In *obe* mutants, the down-regulation of centrosomal γ-tubulin occurred at the same stage and to the same extent as in wild type, even though centrosomes failed to move away from the cortex (Fig. S2, B and C). These results indicate that the defects in *obe* mutants are not caused by increased microtubule nucleating activity at centrosomes, but may instead result from an aberrant association between microtubules and junctional proteins at the cell cortex.

The apical epithelial domain is expanded in *obelus* mutants

The adherens junction defects in *obe* mutants are reminiscent of embryos that lack Par-6 or aPKC, which are associated with the Crumbs apical protein (Blankenship et al., 2006; Harris and Peifer, 2007). To test whether the defects in *obe* mutants are caused by a reduction in the activity of apical complex proteins, we analyzed Crumbs and aPKC localization and activity. Autophosphorylation of aPKC at T567/T574 (corresponding to T555/563 in the human protein), an indicator of kinase activity (Hirai and Chida, 2003), was unchanged in *obe* mutants (Fig. S3 C). In addition, Par-3 phosphorylation at serine 980 (Par-3 phospho-S980), an aPKC target site (Morais-de-Sá et al., 2010), occurred normally (Fig. S3, A and B). Moreover, unlike *aPKC* mutants, in which Crumbs fails to localize to the apical membrane (Harris and Peifer, 2007), Crumbs and aPKC were readily detected at the apical domain in *obe* mutants (Fig. 4, C and D). Similarly, although embryos lacking Crumbs have reduced levels of Par-3 (Morais-de-Sá et al., 2010), Par-3 levels were not affected in *obelus* mutants (Fig. S3 D). These results suggest that the defects in *obe* mutants are not caused by a strong reduction in the activity of apical proteins.

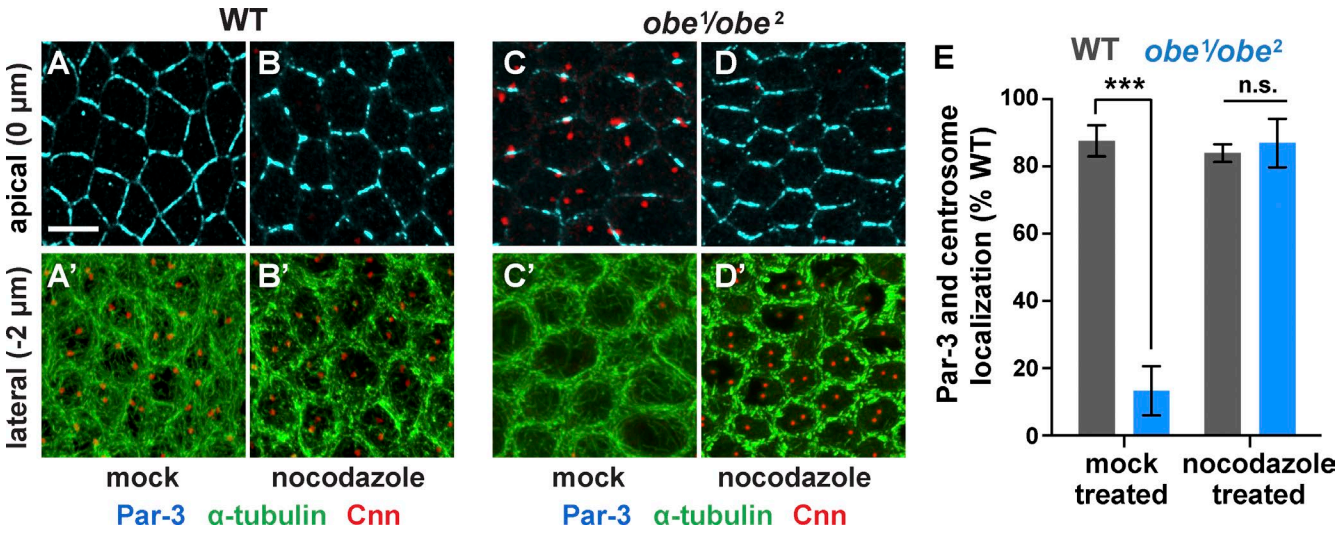

Figure 3. **The junctional and centrosome defects in *obe* mutants are rescued by inhibiting microtubule polymerization.** (A–D) Wild-type (WT) embryos (A and B) and *obe*^{1}/*obe*^{2} mutants (C and D) at stage 7, either mock treated (A and C) or incubated for 7 min in 56-nM nocodazole immediately before fixation (B and D). Centrosomes (Cnn) moved to a lateral position basal to the Par-3 plane, and Par-3 was distributed along horizontal cell interfaces in mock-treated and nocodazole-treated wild-type embryos (n = 7–10 embryos per condition). In untreated *obe* mutants, centrosomes remained in the same plane as Par-3 aggregates. Centrosome positioning and Par-3 localization were restored to wild type in nocodazole-treated *obe* mutants (n = 13–15 embryos per condition). (E) Percentage of embryos with wild-type Par-3 localization (no aggregates) and centrosomes that were correctly positioned laterally. In mock-treated embryos, 87% of *obe* mutants had Par-3 aggregates compared with 11% of wild-type controls (***, P = 0.0008 by unpaired t test). In nocodazole-treated embryos, 13% of *obe* mutants had Par-3 aggregates compared with 16% of wild-type controls (n.s., P = 0.72). Means ± SEM between experiments are shown. The *obe*^{1}/*obe*^{2} mutant embryos were the progeny of *obe*^{1}/*obe*^{2} females crossed to *obe*^{2}/+ males. Anterior left, dorsal up. Bar, 10 µm. See also Fig. S2.

To investigate whether Obelus affects a distinct aspect of apical domain organization or activity, we analyzed the localization of Crumbs and aPKC in *obe* mutants. Crumbs and aPKC are normally localized just apical to and partially overlapping with the adherens junctions in wild type (Fig. 4, A and B; Harris and Peifer, 2005). In contrast, the Crumbs and aPKC domains were expanded to more than twice their usual height along the apical–basal axis in *obe* mutants (Fig. 4, D–H). Together, these results indicate that *obe* mutants do not have a strong loss of aPKC activity or cortical localization. Instead, *obe* mutants display an expansion of the apical epithelial domain.

Obelus is a conserved Ski2-family DExD/H-box helicase

To identify the gene that is responsible for the defects in *obe* mutants, we mapped *obe* to the 88F6–88F7 region on chromosome 3R (Fig. 5 A). The axis elongation, male sterility, and Par-3 aggregation defects in the progeny of *obe*^{1}, *obe*^{1}/*obe*^{2}, and *obe*^{2}/*Df* females were fully rescued by the CH322-15H13 bacterial artificial chromosome (BAC), which covers a 21.6-kb region containing five genes (Fig. 5, A and B; and not depicted). Whole-genome DNA sequencing revealed a 19-bp deletion in the second exon and a point mutation at nucleotide 173 of the CG5205 gene in *obe*^{2} mutants. Together, these changes are predicted to cause a frameshift after amino acid 48 and introduce a stop codon at amino acid 52 of the predicted 2,183–amino acid protein (Fig. 5 C). The CG5205 transcript was expressed at 2% of its wild-type levels in the progeny of *obe*^{2}/*Df* females by quantitative RT-PCR (qRT-PCR) and is unlikely to encode functional protein. We did not identify mutations in exons or splice sites of CG5205 in *obe*^{1}, but the full-length CG5205 transcript was expressed at 10% and 7% of wild-type levels in the progeny of *obe*^{1} and *obe*^{1}/*obe*^{2} females, respectively, by qRT-PCR. Moreover, expression of the CG5205 cDNA from a ubiquitous promoter rescued the axis elongation, male sterility, Par-3 aggregation, and centrosome positioning defects of *obe*^{1} and *obe*^{1}/*obe*^{2} mutants (Fig. 5, B and D–F; and not depicted). These results demonstrate that *obe*^{1} and *obe*^{2} are strong loss-of-function and null mutations, respectively, in the CG5205 gene.

The *obelus*/*CG5205* gene encodes a Ski2-like DExD/H-box helicase, a member of a subclass of superfamily 2 helicases with two tandem helicase domains and two Sec63 domains (Fig. 5, G and H; Johnson and Jackson, 2013). Obelus is highly conserved from yeast to humans, with 55% amino acid identity to human ASCC3 and 45% identity to human SNRNP200. The yeast paralogue Brr2 and the human paralogue SNRNP200 are components of the spliceosome, a large ribonucleoprotein complex that catalyzes the splicing of pre-mRNA transcripts (Lauber et al., 1996; Noble and Guthrie, 1996; Xu et al., 1996). Studies in *Saccharomyces cerevisiae* and human cell lines demonstrate that Brr2 and SNRNP200 promote the ATP-dependent unwinding of RNA duplexes in the spliceosome (Laggerbauer et al., 1998; Raghunathan and Guthrie, 1998; Kim and Rossi, 1999). Although the structure and biochemical activity of Brr2 are well characterized (Zhang et al., 2009; Cordin and Beggs, 2013; Johnson and Jackson, 2013; Mozaffari-Jovin et al., 2013), the physiological functions of this helicase family have not been previously analyzed in a multicellular organism.

Obelus regulates alternative splicing of the *crumbs* pre-mRNA

Based on its homology to the Brr2 and SNRNP200 RNA helicases, we speculated that *obelus* may be required for pre-mRNA splicing or mRNA stability. To test this, we used RNA sequencing to compare the transcriptional and splicing profiles of staged wild-type embryos with *obe*^{1}/*obe*^{2} and *obe*^{2}/*Df* mutants. We focused on transcripts that were differentially expressed or spliced compared with wild type and were equally

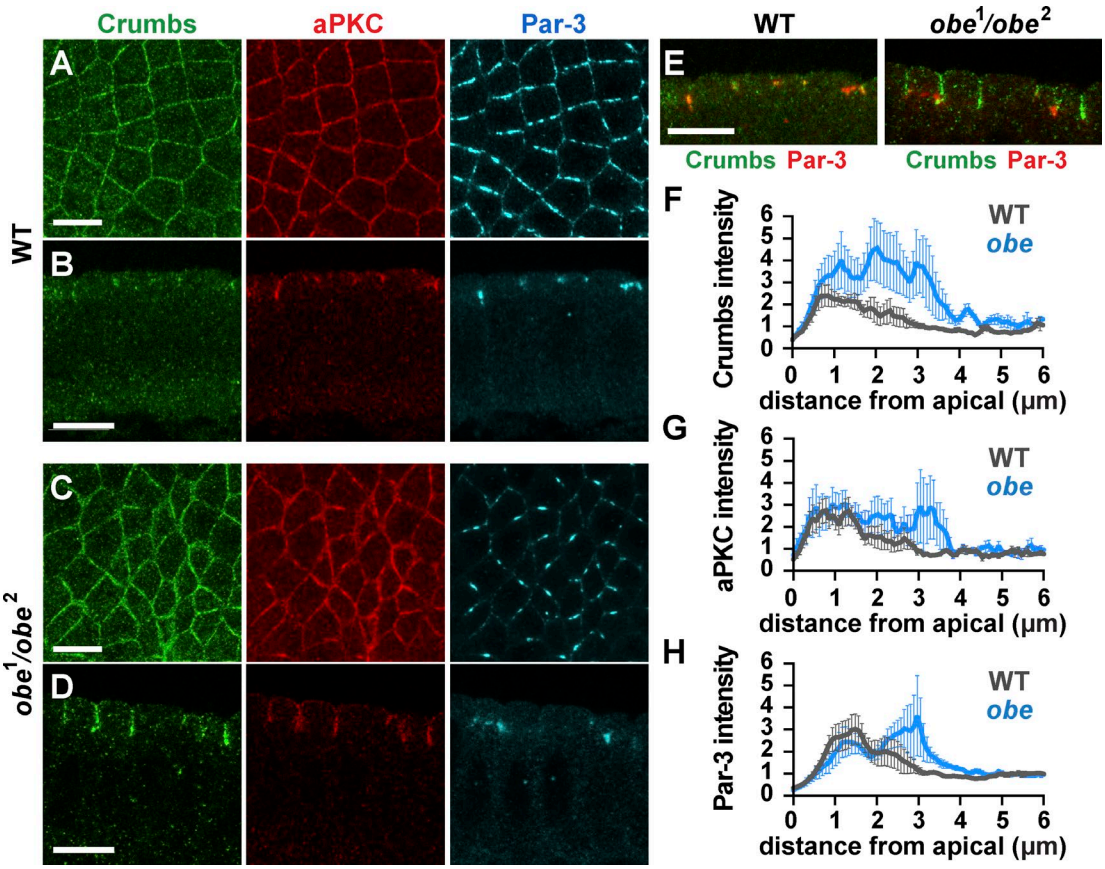

Figure 4. **The apical epithelial domain is expanded in *obe* mutants.** (A–D) Localization of Crumbs, aPKC, and Par-3 in wild-type (WT) and obe^1/obe^2 embryos at stage 7. (E) Merged image of the embryos in B and D showing expansion of the Crumbs apical domain (and the basolateral displacement of Par-3). (F–H) Cortical intensity of Crumbs (F), aPKC (G), and Par-3 (H) along the lateral membrane of wild-type and obe^1/obe^2 embryos in stage 7 (0 µm is the most apical plane). The Crumbs and aPKC domains were expanded in *obe* mutants (0.5–4.0 µm) compared with wild type (0.5–2.0 µm; *n*, four to six embryos per genotype and three to six edges per embryo). Error bars indicate the SEM between embryos. The obe^1/obe^2 mutant embryos were the progeny of obe^1/obe^2 females crossed to obe^2/+ males. (A and C) Anterior left, dorsal up. (B, D, and E) Cross sections, apical up. Bars, 10 µm. See also Fig. S3.

or more severely affected in the stronger obe^2/Df mutant. False positives that could be explained by variations in developmental staging were excluded (see Materials and methods section RNA sequencing). By these criteria, CG5205 was the only transcript that was significantly down-regulated in both *obe* alleles, and five transcripts were significantly up-regulated compared with wild type (Table S1). In addition, 14 transcripts were differentially spliced in both *obe* alleles (Fig. S4). For three genes, *crumbs*, CG4449, and CG32581, splicing changes in *obe* mutants resulted in alterations to the coding region. These results indicate that *obe* is required for the alternative splicing of a small number of transcripts in the early *Drosophila* embryo.

As Crumbs is required for apical–basal polarity and adherens junction organization (Bulgakova and Knust, 2009; Tepass, 2012; Thompson et al., 2013), we focused on Crumbs as a potential target that could mediate the effects of Obelus on epithelial polarity. Four isoforms of Crumbs have been reported in *Drosophila* (dos Santos et al., 2015). Three isoforms (*crumbs-RA*, *crumbs-RB*, and *crumbs-RC*) have been verified by RNA sequencing (Celniker et al., 2009), but only the *crumbs-RA* isoform has been functionally characterized. The predominant isoform in the early embryo, *crumbs-RA*, encodes a transmembrane protein with a large extracellular domain composed of 28 EGF-like repeats and 3 laminin–AG domains (Fig. 6 A; Tepass et al., 1990). The *crumbs-RC* isoform is generated by an alternative splicing event that leads to the inclusion of exon 4, which encodes an additional EGF-like repeat after repeat 7 in the Crumbs extracellular domain (Fig. 6, A and B). Total *crumbs* mRNA levels in *obe* mutants were similar to wild type (Fig. 6, C and D). However, the *crumbs-RC* isoform was dramatically up-regulated at the expense of *crumbs-RA* in *obe* mutants (Fig. 6, C and E). The *crumbs-RC* isoform comprised <20% of total *crumbs* transcripts in wild type, but was >60% of *crumbs* transcripts in obe^1/obe^2 embryos and >80% of *crumbs* transcripts in obe^2/Df embryos (Fig. 6, C and E). These results demonstrate that Obelus is required to generate the *crumbs-RA* isoform that removes exon 4 of the *crumbs* transcript.

Overexpression of Crumbs-PC recapitulates the defects of *obelus* mutants

Crumbs overexpression causes an expansion of the apical domain and a basolateral displacement of adherens junctions in *Drosophila* embryonic and pupal epithelia (Wodarz et al., 1995; Grawe et al., 1996; Pellikka et al., 2002). To test whether the defects in *obe* mutants are caused by increased Crumbs activity, we analyzed the effects of overexpressing Crumbs-PA and Crumbs-PC on apical–basal polarity, junctional organization, and centrosome positioning in the early embryo. Crumbs-PA and Crumbs-PC were expressed at similar levels and localized

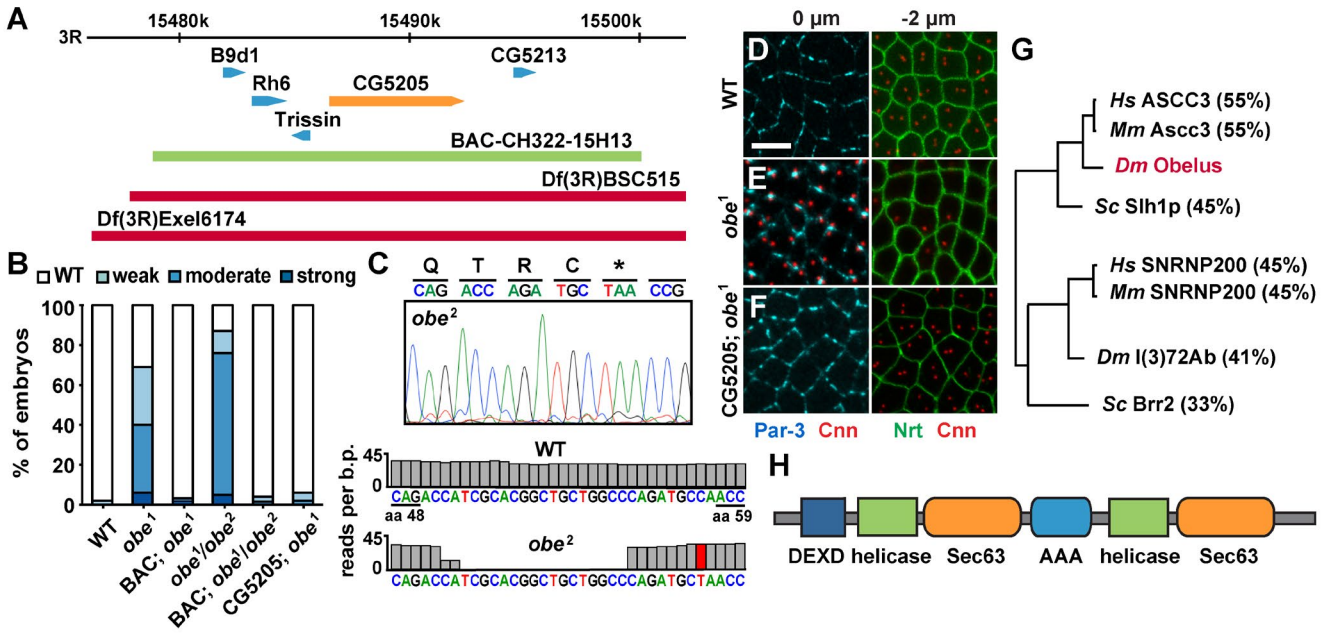

Figure 5. ***Obelus* encodes a predicted Ski2-family DExD/H-box helicase.** (A) The *obe* mutation maps to chromosome 3R. The Df(3R)Exel6174 and Df(3R)BSC515 deficiencies failed to complement the axis elongation defects in the progeny of obe^1 and obe^2 hemizygous females crossed to obe^1/+ males. (B) The CH322-15H13 BAC rescued axis elongation in the progeny of obe^1/obe^1 and obe^1/obe^2 females crossed to obe^1/+ males ($P < 0.0001$ by χ^2 test). Ubiquitous expression of the CG5205 cDNA rescued elongation in the progeny of obe^1 females crossed to obe^1/+ males ($P < 0.0001$; $n = 76–133$ embryos/condition). (C) Sanger sequencing (top) and whole-genome sequencing (bottom) determined that the obe^2 allele contains a 19-bp deletion in the second exon of CG5205 and a C to T point mutation at nucleotide 173. These changes introduce a frameshift after amino acid 48 and a stop codon at amino acid 52 that result in a truncated protein. The asterisk denotes a premature stop codon. The C and A 3′ to the deletion were ambiguously assigned. (D–F) Par-3, centrosomes (Cnn), and lateral membrane marker (Nrt) in wild-type, obe^1, and obe^1 embryos expressing the CG5205 cDNA. In CG5205-expressing embryos, Par-3 does not aggregate and centrosomes relocate correctly to a more basal plane. (G) Phylogenetic tree. There are two closely related paralogues in *S. cerevisiae* (*Sc*), *Drosophila* (*Dm*), mice (*Mm*), and humans (*Hs*; percentage of amino acid identity to CG5205 indicated). (H) CG5205 contains a DExD/H-box domain, two helicase domains, two Sec63 domains, and an AAA^+ ATPase domain. Anterior left, dorsal up. Bar, 10 µm.

to the apical membrane when overexpressed at moderate levels, indicating that these two isoforms do not differ in overall stability or localization (Fig. S5, A and B). Moreover, both Crumbs-PA and Crumbs-PC retain apical-promoting functions, as overexpressing either isoform at high levels produced an expansion of the apical domain and a basolateral displacement of Par-3 (Fig. S5 B).

Overexpression of the two Crumbs isoforms at moderate levels revealed that these isoforms had distinct effects on centrosome positioning and Par-3 localization. More than half of Crumbs-PC–expressing embryos had centrosomes that were apically mislocalized at stage 7 (63 ± 5%, compared with 2 ± 1% in wild type; $P < 0.0001$; Fig. 7, A, C, and F), and more than one third of centrosomes were in close proximity to adherens junctions (38 ± 5%, compared with 1 ± 0.5% in wild type; $P < 0.0001$; Fig. 7 G). In contrast, centrosome localization was only weakly defective in embryos overexpressing Crumbs-PA (10 ± 3% of Crumbs-PA–expressing embryos had apically mislocalized centrosomes, and 6 ± 2% had centrosomes near adherens junctions; Fig. 7, B, F, and G). In contrast, centrosome positioning occurred normally in *crumbs* mutants (Fig. 7 D). These observations, in addition to the expanded apical epithelial domain in *obe* mutants (Fig. 4, D–H), are consistent with the idea that *obe* mutants have increased Crumbs activity.

In addition to distinct effects on centrosome positioning, Crumbs-PA and Crumbs-PC had different effects on Par-3 localization. Moderate overexpression of Crumbs-PC, but not Crumbs-PA, produced a significant proportion of embryos with single, large Par-3 aggregates that resembled *obe* mutants (Fig. 7, C and H). These large Par-3 aggregates were rarely observed in *crumbs* mutants or in embryos overexpressing Crumbs-PA (Fig. 7, B, D, and H). In addition, overexpression of either Crumbs-PA or Crumbs-PC produced a fragmented distribution of Par-3 into many small aggregates at the cell cortex in a dispersed pattern, similar to the defects in *crumbs* mutants (Fig 7, D and I), consistent with the idea that these two isoforms possess partially overlapping activities. Collectively, these results demonstrate that although both isoforms of Crumbs retain some common functions, overexpression of Crumbs-PC, but not Crumbs-PA, causes centrosome positioning and junctional aggregation defects that closely resemble *obe* mutants.

Discussion

Alternative splicing events can have profound consequences for protein function, but few factors have been identified that regulate critical alternative splicing events in vivo. Here, we identify a functional target of the conserved Ski2-family helicase Obelus and show that Obelus is required for junctional organization and centrosome positioning in the *Drosophila* embryo. The loss of Obelus is associated with a failure to exclude exon 4 from the *crumbs* transcript, resulting in a switch in isoform expression from the Crumbs-PA isoform to the Crumbs-PC isoform that contains an additional EGF-like repeat in the extracellular domain. The apical epithelial domain is expanded in *obe* mu-

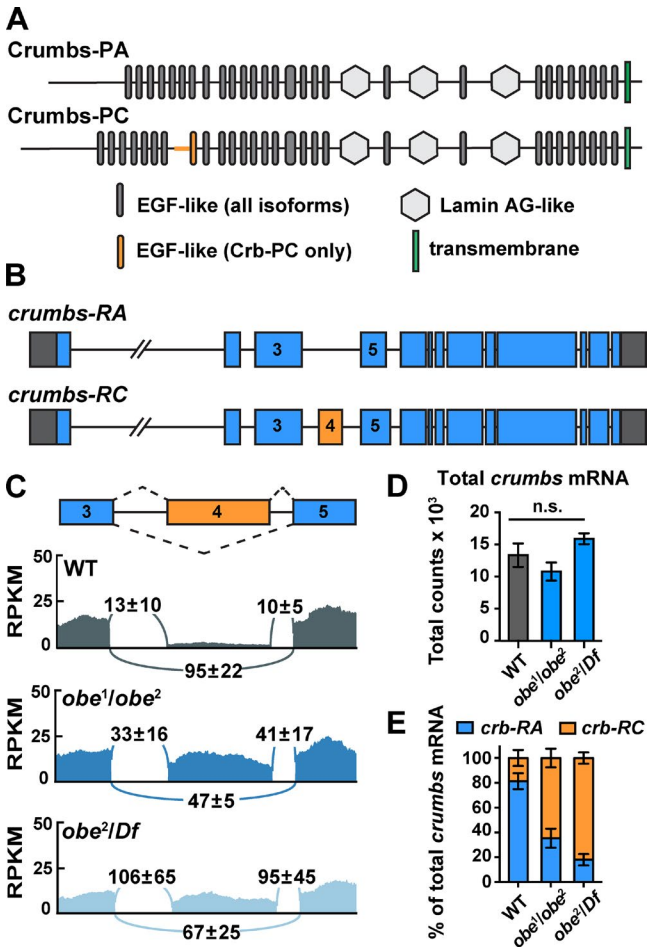

Figure 6. ***Crumbs* alternative splicing is disrupted in *obelus* mutants.** (A) Crumbs-PA contains 28 EGF-like repeats, three lamin AG–like domains, and a transmembrane domain. Crumbs-PC contains an additional EGF-like repeat after repeat 7. (B) Schematics of *crumbs* splice variants expressed in *obe* mutants, numbered according to Flybase (dos Santos et al., 2015). Orange, alternative exon included in *crumbs-RC*. Gray, 5′ and 3′ UTRs. Introns are not to scale. (C) RNA sequencing read density in RPKM (reads per kilobase per million mapped reads) across exon 4 of *crumbs* and its flanking exons in wild-type (WT; gray), obe^1/obe^2 (dark blue), and obe^2/Df (light blue) embryos at late stage 5/early stage 6. (D) Total *crumbs* mRNA levels in wild type (13,352 ± 1,061) were not significantly affected in obe^1/obe^2 (10,800 ± 881.4; P = 0.13) and obe^2/Df (15,905 ± 488.3; P = 0.09). n.s., not significant. (E) The percentage of *crumbs-RA* in wild type (81 ± 4%) is significantly reduced in obe^1/obe^2 (35 ± 4%; P = 0.0013 by unpaired *t* test) and obe^2/Df (18 ± 3%; P = 0.0002 by unpaired *t* test; three biological replicates per condition). Means ± SD (C) or ± SEM (D and E) between biological replicates are shown. The obe^1/obe^2 and obe^2/Df mutant embryos were the progeny of obe^1/obe^2 and $obe^2/Df(3R)Exel6174$ females, respectively, crossed to $obe^2/+$ males. See also Table S1 and Fig. S4.

tants, and the junctional localization and centrosome positioning defects in *obe* mutants are recapitulated by overexpression of the Crumbs-PC but not the Crumbs-PA isoform. These results suggest that the conserved Obelus helicase regulates the activity of the Crumbs apical determinant by inhibiting the expression of a potentially more active form of the protein, providing a mechanism for tuning the size of the epithelial apical domain during development.

We propose that increased or altered activity of the Crumbs-PC isoform triggers a series of events that alter centrosome positioning and junctional organization in *obe* mutants. Crumbs regulates both junctional position along the apical–basal axis and the extent of junctional clustering, and either a strong loss or gain of Crumbs activity disrupts adherens junction organization (Wodarz et al., 1995; Tepass, 1996). Here, we provide evidence that a more subtle modulation of Crumbs activity through the inclusion of an additional EGF repeat in its extracellular domain provides an endogenous mechanism that modulates the effect of Crumbs on junctional regulation. In one model, increased activity of Crumbs-PC could result in excessive exclusion of Par-3 from the cortex. As Crumbs and its associated apical proteins displace Par-3 and adherens junctions from the cortex (Krahn et al., 2010; Morais-de-Sá et al., 2010; Walther and Pichaud, 2010), the apical expansion in *obe* mutants could enhance Par-3 exclusion from the apical cortex and corral the remaining Par-3 protein into a subset of its normal territory (Fig. 7 J). Alternatively, the two isoforms could have distinct functions, for example, if Crumbs-PA inhibits junctional clustering and Crumbs-PC promotes clustering. In both models, increased clustering is predicted to enhance Par-3 oligomerization, which exposes the Par-3 N-terminal domain that binds to and bundles microtubules (Chen et al., 2013). The association between Par-3 and microtubules could drive further junctional aggregation in *obe* mutants, as microtubules enhance adherens junction clustering (Brieher and Yap, 2013). Microtubules could in turn capture and translocate centrosomes to the cortex through the activity of the junction-associated minus end–directed motor dynein (Ligon et al., 2001; Schmoranzer et al., 2009; Kotak et al., 2012). Thus, increased or altered Crumbs activity in *obe* mutants could trigger a cascade of events that lead to Par-3 aggregation and centrosome mispositioning, ultimately disrupting epithelial polarity and junctional remodeling. Microtubule-dependent positive feedback between Par-3 and centrosomes may be important for many processes within cells, including the establishment of apical–basal polarity (Feldman and Priess, 2012; Jiang et al., 2015) and oriented cell division in the stem cell niche (Inaba et al., 2015).

In contrast to Brr2, which regulates the constitutive splicing of most intron-containing genes in *S. cerevisiae* (Pleiss et al., 2007), Obelus is specifically required for the alternative splicing of a relatively small number of transcripts in the early *Drosophila* embryo. This specificity may be the result of differences in the functions of Obelus and Brr2, or an expansion of the mechanisms that regulate alternative splicing in *Drosophila* compared with yeast. Alternative splicing is more commonly used in multicellular organisms, and studies in zebrafish and in human and *Drosophila* cell lines have shown that depleting conserved spliceosome complex proteins, including Brr2, selectively affects only a subset of alternative splicing events (Park et al., 2004; Rösel et al., 2011; Brooks et al., 2015; Wickramasinghe et al., 2015). Here, we combine genome-wide transcriptome analysis with molecular genetic approaches to identify the functional target of a conserved Ski2-family helicase in a multicellular organism in vivo. Collectively, these findings demonstrate that proteins with homology to core components of the splicing machinery in yeast can perform highly tissue- and transcript-specific functions in multicellular organisms. Although the biochemical activities of Obelus and its orthologues have not been extensively characterized, the *S. cerevisiae* Obelus paralogue Brr2 is an RNA helicase that promotes RNA duplex unwinding in the spliceosome, leading to conformational changes that are important for pre-mRNA splicing (Cordin and Beggs, 2013; Johnson and Jackson, 2013). The human Obelus paralogue SNRNP200 has

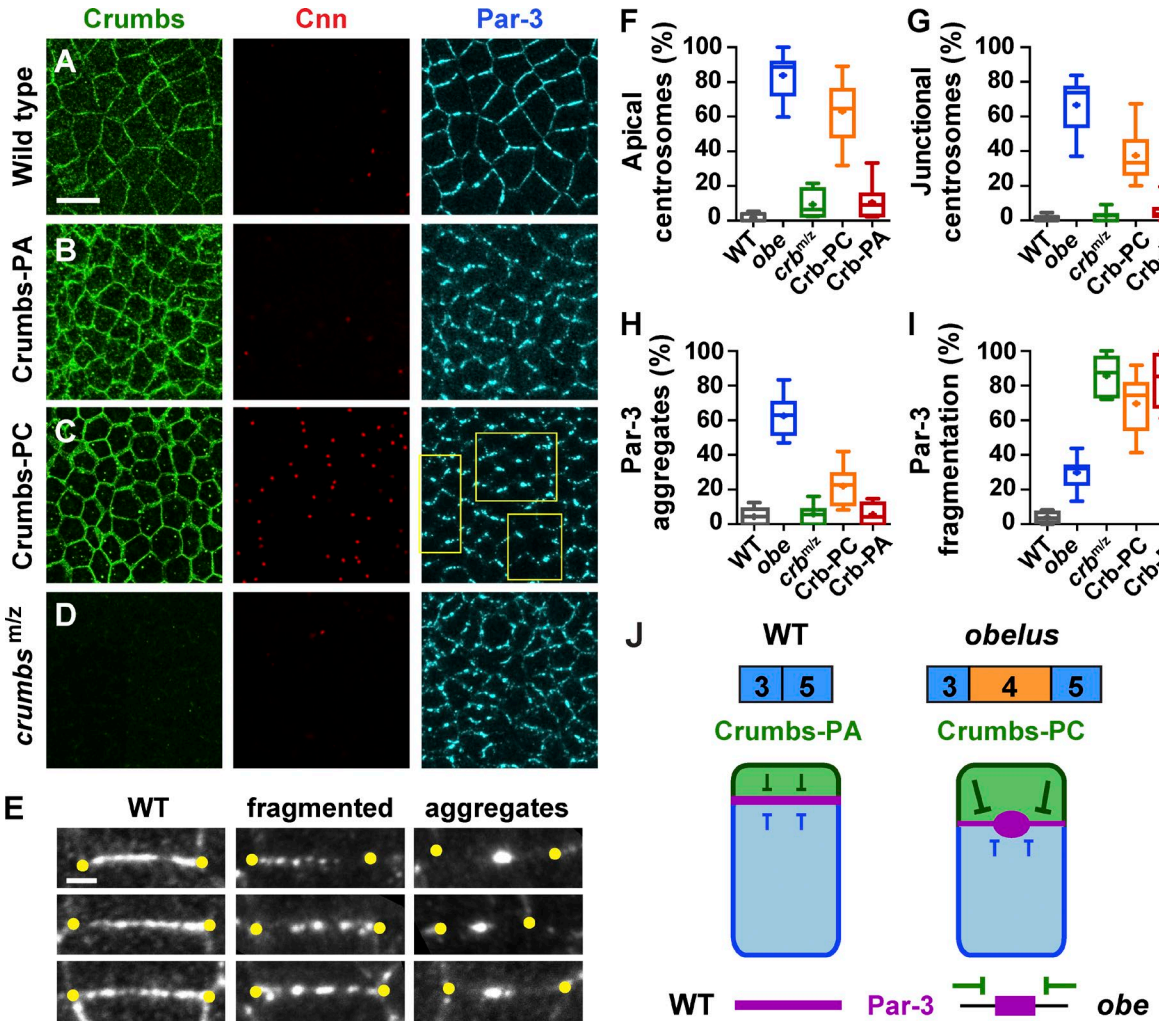

Figure 7. **Crumbs overexpression recapitulates the cell polarity defects of *obe* mutants.** (A–D) Localization of Crumbs (anti-Crumbs antibody), centrosomes (Cnn), and Par-3 in wild type (A), embryos overexpressing Crumbs-PA (B) or Crumbs-PC (C), and *crumbs*^{11A22} maternal and zygotic mutants (*crumbs*$^{m/z}$; D). All embryos are stage 7. Gal4/+ was the wild-type control. Moderate overexpression of Crumbs-PC induced Par-3 aggregation and centrosome mispositioning compared with wild type. Yellow boxes in C highlight representative cell interfaces. (E) Examples of edges with wild type (WT), fragmented, or aggregated Par-3 (white) localization. Left, examples from wild-type embryos. Middle and right, top example from Crumbs-PA and bottom two examples from Crumbs-PC. Yellow dots mark the endpoints of cell interfaces. (F) The percentage of apically mispositioned centrosomes was significantly increased in *obe*^{1}/*obe*^{2} mutants ($P < 0.0001$) and in embryos overexpressing Crumbs-PC ($P < 0.0001$ by unpaired *t* test). Apically mispositioned centrosomes occurred to a lesser extent in *crb* mutants ($P = 0.01$) and Crumbs-PA–expressing embryos ($P = 0.02$). (G) The percentage of centrosomes in close proximity to adherens junctions was significantly increased in embryos overexpressing Crumbs-PC ($P < 0.0001$) and increased to a lesser extent in embryos overexpressing Crumbs-PA ($P = 0.04$). (H) The percentage of Par-3–positive edges with single Par-3 aggregates was significantly increased in embryos overexpressing Crumbs-PC ($P = 0.0004$), but was not affected in *crb* mutant or Crumbs-PA–expressing embryos ($P > 0.5$). (I) The percentage of Par-3–positive edges with Par-3 fragmentation was significantly increased in embryos expressing Crumbs-PC, Crumbs-PA, and *crumbs*$^{m/z}$ mutants ($P < 0.0001$). Boxes, 25–75th percentile. Whiskers, 5–95th percentile. Horizontal line, median. +, mean. Plot shows the distribution of mean values across embryos (19–49 cells analyzed per embryo in 6–10 embryos per genotype). The *obe* mutant embryos were the progeny of *obe*^{1}/*obe*^{2} females crossed to *obe*^{2}/+ males. (J) Model. A switch in isoform expression of the *crumbs* pre-mRNA in *obelus* mutants causes Par-3 aggregation, disrupting adherens junction localization and epithelial remodeling. Anterior left, dorsal up. Bars: (A–D) 10 µm; (E) 2 µm. See also Fig. S5.

also been shown to function as an RNA helicase, and mutations that disrupt its helicase activity are associated with retinal degeneration (Zhao et al., 2009; Santos et al., 2012). These results suggest that Obelus may function as an RNA helicase, although whether Obelus regulates *crumbs* splicing directly or indirectly by controlling other RNA processing or unwinding events that are important for epithelial polarity remains to be determined. In addition, the inability of Crumbs-PC overexpression to fully recapitulate the defects in *obe* mutants could indicate the presence of other RNA targets or other functions of Obelus.

Mutations in the human paralogues of Crumbs and Obelus, CRB1 and SNRNP200, are associated with retinitis pigmentosa, a disease that causes progressive degeneration of retinal photoreceptor cells in humans, leading to blindness (den Hollander et al., 1999; Zhao et al., 2009; Daiger et al., 2013). The identification of Crumbs as a functional target of the Obelus helicase suggests a functional link between these proteins in regulating epithelial organization and integrity. Although previous work on Crumbs has focused on the role of its cytoplasmic domain, our results indicate an important role for the extracellular domain of Crumbs in epithelial polarization and remodeling. In *obelus* mutants, early embryos express increased levels of the Crumbs-PC isoform that contains an additional EGF-like repeat in the extracellular domain. How these two Crumbs isoforms

differ mechanistically remains to be resolved. EGF repeats are present in many proteins involved in cell signaling, polarity, and adhesion, including Notch, Delta, Celsr/Flamingo, and several cadherins. Individual EGF repeats can have profound effects on cell adhesion (Balzar et al., 2001) and ligand–receptor interactions (Rebay et al., 1991) and can influence protein localization and activity by targeting proteins for glycosylation (Acar et al., 2008). The inclusion of an additional EGF repeat in the Crumbs extracellular domain could alter its ability to mediate interactions between cells, as Crumbs homologues promote homophilic adhesion in culture (Zou et al., 2012; Letizia et al., 2013) and the Crumbs extracellular domain is required for its effects on cell polarity, sorting, and survival in vivo (Fletcher et al., 2012; Hafezi et al., 2012; Röper, 2012; Letizia et al., 2013). Crumbs isoforms that differ in the number of EGF repeats have been reported in mice (Mehalow et al., 2003), zebrafish (Zou et al., 2012), and humans (Pruitt et al., 2014), and mutations located within the EGF repeats of the human CRB1 protein are associated with retinitis pigmentosa (den Hollander et al., 1999; Bujakowska et al., 2012). An important goal for further studies will be to determine how inputs that control the structure or activity of the Crumbs extracellular domain influence its essential roles in epithelial organization during normal development and human disease.

Materials and methods

Fly stocks and genetics

Oregon-R was the wild-type control unless otherwise specified. Embryos were raised and scored at 25°C. The *obe*^{1} mutation was isolated in the background of a subset of *piggyBac* insertions on 3R (Schuldiner et al., 2008), and the *obe*^{2} mutation was identified as linked to the *d04274* P-element insertion (Thibault et al., 2004). Precise excision of the transposable elements did not revert the mutant phenotype, which was mapped by deficiency mapping to a different location on chromosome 3R. Both *obe*^{1} and *obe*^{2} failed to complement *Df(3R)Exel6174* (Parks et al., 2004) and *Df(3R)BSC515* (Bloomington *Drosophila* Stock Center; Cook et al., 2012). In all figures except Fig. S1, *obe*^{1}/*obe*^{2} mutants and *obe*^{2}/*Df* mutant embryos were the progeny of *obe*^{1}/*obe*^{2} and *obe*^{2}/*Df(3R)Exel6174* females, respectively, crossed to *obe*^{2}/+ males. The *obe*^{1}/*obe*^{1} and *obe*^{1}/*Df* mutant embryos were the progeny of *obe*^{1}/*obe*^{1} and *obe*^{1}/*Df(3R)Exel6174* females, respectively, crossed to *obe*^{1}/+ males.

Embryos overexpressing Crumbs-PA or Crumbs-PC at moderate levels were the F2 progeny of *UASp–crumbs-PA* or *UASp–crumbs-PC* males × matαtub15 Gal4 females. Embryos overexpressing Crumbs-PA or Crumbs-PC at high levels were the F2 progeny of *UASp–crumbs-PA* or *UASp–crumbs-PC* males × matαtub67;15 Gal4 females (gifts of D. St. Johnston, University of Cambridge, Cambridge, England, UK). Untagged *crumbs* transgenes were used in all experiments except Fig. S5 A, in which GFP-tagged *crumbs* transgenes were used. The *crb*^{11A22} (Tepass et al., 1990) germline clones were generated with the FLP recombinase-dominant female sterile system using FRT82B *ovo*^{D2} (Chou and Perrimon, 1996).

To generate *crumbs* mutant embryos, larvae of the genotype hs-flp/+;FRT82B*crb*^{11A22}/FRT82B *ovo*^{D2} were heat shocked and crossed to FRT82B*crb*^{11A22}/TM3, twi-Gal4, upstream activator sequence (UAS)–GFP males. Homozygous mutant embryos were identified by the absence of GFP from twi-*Gal4*, UAS-*GFP* balancers in embryos sorted before fixation on a fluorescence stereomicroscope (MZFLII; Leica). All GFP-negative embryos were maternally and zygotically mutant for *crb*^{11A22} (referred to as *crb*$^{m/z}$ or *crumbs*$^{m/z}$ in the figures).

Time-lapse imaging

Time-lapse confocal imaging was performed with Resille:GFP (a gift of A. Debec, Institut Jacques Monod, Paris, France). Embryos were dechorionated for 2 min in 50% bleach, washed in water, mounted on an oxygen-permeable membrane (YSI Incorporated) with halocarbon oil 27 (Sigma-Aldrich), and imaged on a spinning-disk confocal microscope (UltraView RS5; PerkinElmer) with a Plan Neofluor 40×, 1.3 NA objective (Carl Zeiss). Z stacks were acquired at 1-µm steps at 15-s intervals. Maximum intensity projections of 2–3 µm in the apical junctional domain were analyzed. Germband length was measured as the long axis of an ellipse fit to the group of cells tracked using custom software in MATLAB (MathWorks; Simões et al., 2010) and was normalized to the value at the onset of elongation at t = 0 in early stage 7. The p-values were calculated using the F-test followed by the appropriate *t* test (using the *t* = 30-min value as the test statistic).

For bright-field imaging, embryos were analyzed 30 min and 3 h after the cellular blastoderm stage under halocarbon oil 27 without dechorionation. Weakly defective *obe* mutants had reduced elongation at 30 min but were indistinguishable from wild type after 3 h. The germband reached 30–40% egg length by 30 min in moderately defective *obe* mutants and <20% egg length by 30 min in strongly defective *obe* mutants and did not recover by 3 h in either case.

Transgenic lines

To generate *sqh-CG5205*, the full-length (6,970 nt) *CG5205* coding sequence was amplified from the CH322-15H13 BAC (BACPAC Resources; Venken et al., 2009) using the following primers: CG5205F, 5′-CAACATGTGGGAGCCGCCACGATTG-3′; and CG5205R, 5′-TTAGACTTCTTTTGCATCAATG-3′. The PCR product was cloned into the *pENTR/D TOPO* vector (Invitrogen), recombined into the *pSqh-GFP-W-attB* destination vector (a gift of F. Wirtz-Peitz, Harvard Medical School, Boston, MA) using the Gateway system (Invitrogen), and inserted into attP40 on chromosome 2 (Genetic Services). For *pEntr-crumbs-PA* and *pEntr-crumbs-PC*, the 5′ portion of the gene containing exons 1–3 of the *crumbs* gene was amplified from *UASt-crumbs*^{WT} (a gift of D. ter Stal and U. Tepass, University of Toronto, Toronto, Canada) using the primers 5′-CCGCGGCCGCCCCCTTCA CCATGGCTAAAATCGCCAATGC-3′ (both), 5′-AGTTGTAA CCCGATGAGCCTGGCTTAC-3′ (PA), and 5′-CCAATGGGGCCCG ATGAGCCTGGCTTAC-3′ (PC). The 3′ portion of the gene containing exons 5–14 was amplified using the primers 5′-CTCATCGGGTTAC AACTGTCAAACGAG-3′ (PA), 5′-GGATACACAGGTTACAAC TGTCAAACGAG-3′ (PC), and 5′-GGGTCGGCGCGCCCACCC TTCTAAATTAGTCGCTCTTCCG-3′ (both). Exon 4 (unique to the PC isoform) was amplified with the primers 5′-GGCTCATCGGGCC CCATTGGTCACTGCC-3′ and 5′-CAGTTGTAACCTGTGTAT CCACTAGCACAAATACAG-3′. The vector *pEntr* was amplified using the primers 5′-AAGGGTGGGCGCGCCGAC-3′ and 5′-GGT GAAGGGGGCGGCCGC-3′. For *pEntr-GFP:crumbs-PA* and *pEntr -GFP:crumbs-PC*, an internal GFP tag (starting at amino acid 89) plus exons 1–3 was amplified from *UASt-GFP:crumbs* (gift of D. ter Stal and U. Tepass) using the primers above. The exons 1–3, exons 5–14, and pEntr fragments were assembled into *pEntr-crumbs-PA* and *pEntr-GFP:crumbs-PA*, and the exons 1–3, exon 5, exons 5–14, and pEntr fragments were assembled into *pEntr-crumbs-PC* and *pEntr -GFP:crumbs-PC* using the Gibson Assembly Master Mix (New England Biolabs, Inc.) and grown in DH5α chemically competent *Escherichia coli*. The *pEntr-GFP:crumbs-PA* and *pEntr-GFP:crumbs -PC* constructs were assembled with the same method using the exon 1–3:GFP fragment. All *crumbs* constructs were recombined into the pUASp-W-attB destination vector (gift of M. Buszczak, University of Texas Southwestern Medical Center, Dallas, TX) to generate

pUASp-crumbs-PA, *pUASp-crumbs-PC*, *pUASp-GFP:crumbs-PA*, and *pUASp-GFP:crumbs-PC*. All transgenes were inserted in VK37 on chromosome 2. The CH322-15H13 genomic BAC clone (BAC PAC Resources; Venken et al., 2009) was prepped using the Large-Construct kit (QIAGEN), and the transgene was inserted into attP40 on chromosome 2 (Genetic Services).

Immunohistochemistry

Embryos were dechorionated for 2 min in 50% bleach and washed with water. Primary antibodies were rabbit aPKC (1:500; Santa Cruz Biotechnology, Inc.), rabbit β-catenin (1:200; Riggleman et al., 1990), rabbit centrosomin (1:500; Lucas and Raff, 2007), mouse Crumbs (1:2; Developmental Studies Hybridoma Bank [DSHB]), rat E-cadherin (1:25; DSHB), mouse neurotactin (1:200; DSHB), guinea pig Par-3/Bazooka (1:500; Blankenship et al., 2006), rabbit Par-3 phospho-S980 (1:250; Krahn et al., 2009), mouse α-tubulin (1:1,000; DM1α; Sigma-Aldrich), and mouse γ-tubulin (1:1,000; Martinez-Campos et al., 2004). For immunostaining with antibodies to β-catenin, Par-3, Crumbs, and neurotactin, embryos were boiled for 10 s in 0.03% Triton X-100/0.4% NaCl, cooled on ice for >30 min, and devitellinized in heptane/methanol. For antibodies to E-cadherin and aPKC, embryos were fixed for 1 h in 4% paraformaldehyde in 0.1-M sodium phosphate buffer and manually devitellinized. For α-tubulin, embryos were fixed for 10 min in 10:9:1 heptane, 37% paraformaldehyde, and 0.5-M EGTA and manually devitellinized. For all other antibodies, embryos were fixed for 20 min in 4% formaldehyde in PBS/heptane and devitellinized in heptane/methanol. Secondary antibodies conjugated to Alexa Fluor 488, 568, or 647 (Molecular Probes) were used at 1:500. Embryos were mounted in Prolong Gold (Invitrogen), imaged on a confocal microscope (LSM700; Carl Zeiss) with a PlanApo 40× 1.4 NA objective (1-µm optical sections acquired at 0.5-µm steps), and staged by posterior midgut morphology.

Western blots

The expression levels of the *pUASp-GFP:crumbs-PA* and *pUASp-GFP:crumbs-PC* transgenes were compared by Western blot analysis. Embryos expressing the respective UASp transgenes under the control of matαtub15 Gal4 were subjected to Western blot analysis using standard procedures. Late stage 5/early stage 6 embryos were lysed in a sample buffer and boiled for 5 min. Equal amounts of embryonic lysate per lane were run on a 4–12% (vol/vol) Bis-Tris SDS/PAGE gel or 4% Tris-acetate SDS-PAGE gel (NuPAGE; Invitrogen). Protein was transferred to a 0.45-µm nitrocellulose membrane by standard protocols. Primary antibodies were used at the following concentrations: rabbit GFP (1:1,000; Torrey Pines), rabbit phospho-aPKC T555/T563 (these sites on the human protein correspond to T567/T574 in *Drosophila* aPKC isoform PA; 1:1,000; 5813; Abcam), mouse α-tubulin (DM1α; 1:1,000; Sigma-Aldrich), and guinea pig Par-3 (1:1,500; Blankenship et al., 2006). Secondary antibodies were mouse, rabbit, and guinea pig HRP-conjugated antibodies (1:10,000; Jackson ImmunoResearch Laboratories, Inc.) and were detected by chemiluminescence imaging (ECL Plus Western Blotting Detection Reagents; GE Healthcare). For phospho-aPKC (T555/T563) and total Par-3 level analysis, Oregon-R was the wild-type control, and obe^1/obe^2 mutant embryos were the progeny of obe^1/obe^2 females crossed to obe^2/+ males.

Nocodazole treatment

Oregon-R and obe^1/obe^2 embryos were shaken at 220 rpm for 7 min in 1:1 PBS/heptane in the presence or absence of 56-nM nocodazole. After nocodazole treatment, embryos were fixed immediately in 100 ml of 0.5-M EGTA, 900 ml of 37% formaldehyde solution, and 1 ml heptane, shaken at 220 rpm for 10 min, and manually devitellinized.

Whole-genome sequencing

Genomic DNA was isolated from wild-type, obe^1/obe^1, and obe^2/Df adult males and sequenced using paired-end SOLiD (Sequencing by Oligonucleotide Ligation and Detection) whole-genome sequencing technology (Applied Biosystems). Sequenced libraries were mapped to the *Drosophila* genome (DM3; UCSC) using a custom pipeline generated by N. Socci at the Memorial Sloan Kettering Cancer Center Bioinformatics core facility. The wild-type control was the starting chromosome on which the obe^1 mutation arose (Schuldiner et al., 2008). No such chromosome was available for obe^2, but the identified obe^2 mutations were not present in this control or in Oregon-R.

qRT-PCR

Total RNA was isolated from late stage 5/early stage 6 Oregon-R, obe^1/obe^1, obe^1/obe^2, and $obe^2/Df(3R)Exel6174$ embryos as described in the next section. For each sample, 1 µg of total RNA was DNase treated and then reverse transcribed using the High Capacity cDNA Reverse Transcription kit (Applied Biosystems). Then, 50 ng cDNA was amplified in each qRT-PCR reaction using predesigned TaqMan gene expression assays for exons 5 and 6 of *CG5205* (Dm02140819_g1) and exons 2 and 3 of *RpL32* (Dm02151827_s1; Applied Biosystems). Reactions were carried out using a 7900HT Fast Real-Time PCR system (Applied Biosystems). Relative expression levels were quantified using the $2^{-\Delta\Delta C(T)}$ method (Schmittgen and Livak, 2008), and expression was normalized to *RpL32* within each sample. The results are the means of three technical replicates.

RNA sequencing

Genotypes used for RNA sequencing were Oregon-R, obe^1/obe^2, and $obe^2/Df(3R)Exel6174$, three biological replicates for each genotype. Total RNA was extracted from ~50 embryos hand selected at late stage 5/early stage 6 using the TRIzol (Invitrogen) extraction protocol. RNA sequencing was carried out by the New York Genome Center using the HiSeq2500 platform (Illumina) with 50-bp paired-end reads and >20 million reads per sample. Sequenced libraries were mapped to the *Drosophila* genome (DM3; UCSC Genome Browser) using the RNA-Seq aligner STAR (v_2.3.1z). Differential analysis of gene and transcript expression was performed using Cuffdiff 2 (v_cufflinks-2.1.1; Trapnell et al., 2013). Transcripts that were differentially expressed in both mutant samples compared with wild type, were similarly or more strongly affected in the stronger obe^2/Df combination, and had ≥30 reads in all samples were selected for further analysis. Analysis of several maternally and zygotically expressed genes (De Renzis et al., 2007; Celniker et al., 2009) revealed that obe^2/Df and obe^1/obe^2 samples were developmentally younger than controls. Transcripts whose differences could be explained by the fact that mutant embryos were slightly younger were excluded from analysis. The complete RNA sequencing data set has been deposited in the Gene Expression Omnibus (accession code GSE74545).

Image analysis

To quantify the localization of Crumbs, aPKC, and Par-3, mean intensity values along line scans from single confocal cross sections were measured using the ImageJ (National Institutes of Health) Plot Profile function with a line width of 0.8 microns. Crumbs, aPKC, and Par-3 intensity was the ratio of the mean pixel intensity along a line scan at the cell boundary relative to the mean intensity of three nonoverlapping cytoplasmic regions of 0.8 microns by 2.4 microns each. A single value was obtained for each image by averaging three to six cell interfaces per image; one to three images in four to six embryos were analyzed per genotype.

Par-3 planar polarity was measured in Scientific Image Segmentation and Analysis (SIESTA) software (Fernandez-Gonzalez and Zal-

len, 2011) and occurred normally in *obe* mutants. We measured the ratio of the mean Par-3 fluorescence intensity at the dorsal and ventral edges (oriented at 0–15° relative to the anterior–posterior axis) to the mean intensity at the anterior and posterior edges (oriented at 75–90°). Cytoplasmic intensity (the mean of all pixels >1 µm from a cell interface) was subtracted from both values before calculating the ratio. P-values were calculated using the F-test followed by the appropriate *t* test.

To quantify the level of γ-tubulin at centrosomes, centrosomes were automatically identified in maximum intensity image projections of a 3-µm-thick region along the apical–basal axis using Otsu thresholding (Otsu, 1979) in ImageJ. The fluorescence intensity of γ-tubulin was measured at each centrosome using the Analyze Particles function in ImageJ. The γ-tubulin intensity was the ratio of the mean intensity of γ-tubulin relative to the mean intensity of all pixels outside of centrosomes. A single value was obtained at each stage by averaging 100–200 centrosomes per image; one to three images in four to seven embryos were analyzed for each genotype. P-values were calculated using the F-test followed by the appropriate *t* test.

To quantify placement of centrosomes in embryos overexpressing Crumbs-PA or Crumbs-PC, centrosomes were identified in maximum intensity image projections of the adherens junctions domain (1.5–2.5 µm) along the apical–basal axis using Otsu thresholding (Otsu, 1979) in ImageJ. Centrosomes were classified as located near the cortex if the shortest distance from the centrosome to the cortex was <1 µm. A single percentage of apically or junctionally localized centrosomes was calculated for each embryo, and plots show the mean values across embryos. P-values were calculated using the F-test followed by the appropriate *t* test.

Online supplemental material

Fig. S1 shows the defects in multiple *obe* allelic combinations. Fig. S2 shows that normal down-regulation of pericentriolar material occurs in *obe* mutants. Fig. S3 shows Par-3 protein levels and Par-3 and aPKC phosphorylation in wild-type and *obe* mutants. Fig. S4 shows sashimi plots and isoform analysis for all transcripts with alternative splicing defects in *obe* mutants. Fig. S5 shows the level of expression and cross sections of embryos that overexpress Crumbs-PA or Crumbs-PC. Table S1 shows all transcripts that were up-regulated or down-regulated more than twofold in *obe* mutants. Online supplemental material is available at http://www.jcb.org/cgi/content/full/jcb.201504083/DC1.

Acknowledgments

We are grateful to Masako Tamada and Justin Sanny for help with the genetic screen that identified *obelus*, Nick Socci at Memorial Sloan Kettering Cancer Center and Nicolas Robine at the New York Genome Center for assistance with sequence analysis, Frederik Wirtz-Peitz for the *pSqh-GFP-W-attB* destination vector, David ter Stal and Ulrich Tepass for the *pUASt-Crumbs*^{WT} and *pUASt-GFP:Crumbs* plasmids, Mike Buszczak for the *pUASp-W-attB* plasmid, and Kathryn Anderson, Mary Baylies, Eric Brooks, Hiten Madhani, Adam Paré, German Sabio, Beate Schwer, and Naomi Stevens for helpful discussions and comments on the manuscript.

This work was supported by National Institutes of Health/National Institute of General Medical Sciences R01 grant GM079340 to J.A. Zallen and by National Institutes of Health T32 training grant GM008539 to A. Vichas. J.A. Zallen is an Investigator of the Howard Hughes Medical Institute.

The authors declare no competing financial interests.

Submitted: 17 April 2015
Accepted: 29 October 2015

References

Acar, M., H. Jafar-Nejad, H. Takeuchi, A. Rajan, D. Ibrani, N.A. Rana, H. Pan, R.S. Haltiwanger, and H.J. Bellen. 2008. Rumi is a CAP10 domain glycosyltransferase that modifies Notch and is required for Notch signaling. *Cell.* 132:247–258. http://dx.doi.org/10.1016/j.cell.2007.12.016

Adams, C.L., Y.T. Chen, S.J. Smith, and W.J. Nelson. 1998. Mechanisms of epithelial cell–cell adhesion and cell compaction revealed by high-resolution tracking of E-cadherin–green fluorescent protein. *J. Cell Biol.* 142:1105–1119. http://dx.doi.org/10.1083/jcb.142.4.1105

Balzar, M., I.H. Briaire-de Bruijn, H.A. Rees-Bakker, F.A. Prins, W. Helfrich, L. de Leij, G. Riethmüller, S. Alberti, S.O. Warnaar, G.J. Fleuren, and S.V. Litvinov. 2001. Epidermal growth factor-like repeats mediate lateral and reciprocal interactions of Ep-CAM molecules in homophilic adhesions. *Mol. Cell. Biol.* 21:2570–2580. http://dx.doi.org/10.1128/MCB.21.7.2570-2580.2001

Bilder, D., M. Schober, and N. Perrimon. 2003. Integrated activity of PDZ protein complexes regulates epithelial polarity. *Nat. Cell Biol.* 5:53–58. http://dx.doi.org/10.1038/ncb897

Blankenship, J.T., S.T. Backovic, J.S. Sanny, O. Weitz, and J.A. Zallen. 2006. Multicellular rosette formation links planar cell polarity to tissue morphogenesis. *Dev. Cell.* 11:459–470. http://dx.doi.org/10.1016/j.devcel.2006.09.007

Blankenship, J.T., M.T. Fuller, and J.A. Zallen. 2007. The *Drosophila* homolog of the Exo84 exocyst subunit promotes apical epithelial identity. *J. Cell Sci.* 120:3099–3110. http://dx.doi.org/10.1242/jcs.004770

Brieher, W.M., and A.S. Yap. 2013. Cadherin junctions and their cytoskeleton(s). *Curr. Opin. Cell Biol.* 25:39–46. http://dx.doi.org/10.1016/j.ceb.2012.10.010

Brooks, A.N., M.O. Duff, G. May, L. Yang, M. Bolisetty, J. Landolin, K. Wan, J. Sandler, B.W. Booth, S.E. Celniker, et al. 2015. Regulation of alternative splicing in *Drosophila* by 56 RNA binding proteins. *Genome Res.* 25:1771–1780. http://dx.doi.org/10.1101/gr.192518.115

Brown, J.B., N. Boley, R. Eisman, G.E. May, M.H. Stoiber, M.O. Duff, B.W. Booth, J. Wen, S. Park, A.M. Suzuki, et al. 2014. Diversity and dynamics of the *Drosophila* transcriptome. *Nature.* 512:393–399. http://dx.doi.org/10.1038/nature12962

Bujakowska, K., I. Audo, S. Mohand-Saïd, M.E. Lancelot, A. Antonio, A. Germain, T. Léveillard, M. Letexier, J.P. Saraiva, C. Lonjou, et al. 2012. *CRB1* mutations in inherited retinal dystrophies. *Hum. Mutat.* 33:306–315. http://dx.doi.org/10.1002/humu.21653

Bulgakova, N.A., and E. Knust. 2009. The Crumbs complex: from epithelial-cell polarity to retinal degeneration. *J. Cell Sci.* 122:2587–2596. http://dx.doi.org/10.1242/jcs.023648

Cavey, M., M. Rauzi, P.F. Lenne, and T. Lecuit. 2008. A two-tiered mechanism for stabilization and immobilization of E-cadherin. *Nature.* 453:751–756. http://dx.doi.org/10.1038/nature06953

Celniker, S.E., L.A. Dillon, M.B. Gerstein, K.C. Gunsalus, S. Henikoff, G.H. Karpen, M. Kellis, E.C. Lai, J.D. Lieb, D.M. MacAlpine, et al. modENCODE Consortium. 2009. Unlocking the secrets of the genome. *Nature.* 459:927–930. http://dx.doi.org/10.1038/459927a

Chen, S., J. Chen, H. Shi, M. Wei, D.R. Castaneda-Castellanos, R.S. Bultje, X. Pei, A.R. Kriegstein, M. Zhang, and S.H. Shi. 2013. Regulation of microtubule stability and organization by mammalian Par3 in specifying neuronal polarity. *Dev. Cell.* 24:26–40. http://dx.doi.org/10.1016/j.devcel.2012.11.014

Chou, T.B., and N. Perrimon. 1996. The autosomal FLP-DFS technique for generating germline mosaics in *Drosophila melanogaster*. *Genetics.* 144:1673–1679.

Cook, R.K., S.J. Christensen, J.A. Deal, R.A. Coburn, M.E. Deal, J.M. Gresens, T.C. Kaufman, and K.R. Cook. 2012. The generation of chromosomal deletions to provide extensive coverage and subdivision of the *Drosophila melanogaster* genome. *Genome Biol.* 13:R21. http://dx.doi.org/10.1186/gb-2012-13-3-r21

Cordin, O., and J.D. Beggs. 2013. RNA helicases in splicing. *RNA Biol.* 10:83–95. http://dx.doi.org/10.4161/rna.22547

Daiger, S.P., L.S. Sullivan, and S.J. Bowne. 2013. Genes and mutations causing retinitis pigmentosa. *Clin. Genet.* 84:132–141. http://dx.doi.org/10.1111/cge.12203

den Hollander, A.I., M.A. van Driel, Y.J. de Kok, D.J. van de Pol, C.B. Hoyng, H.G. Brunner, A.F. Deutman, and F.P. Cremers. 1999. Isolation and mapping of novel candidate genes for retinal disorders using suppression

subtractive hybridization. *Genomics.* 58:240–249. http://dx.doi.org/10.1006/geno.1999.5823

De Renzis, S., O. Elemento, S. Tavazoie, and E.F. Wieschaus. 2007. Unmasking activation of the zygotic genome using chromosomal deletions in the *Drosophila* embryo. *PLoS Biol.* 5:e117. http://dx.doi.org/10.1371/journal.pbio.0050117

dos Santos, G., A.J. Schroeder, J.L. Goodman, V.B. Strelets, M.A. Crosby, J. Thurmond, D.B. Emmert, and W.M. Gelbart. FlyBase Consortium. 2015. FlyBase: introduction of the *Drosophila melanogaster* Release 6 reference genome assembly and large-scale migration of genome annotations. *Nucleic Acids Res.* 43:D690–D697. http://dx.doi.org/10.1093/nar/gku1099

Faustino, N.A., and T.A. Cooper. 2003. Pre-mRNA splicing and human disease. *Genes Dev.* 17:419–437. http://dx.doi.org/10.1101/gad.1048803

Feldman, J.L., and J.R. Priess. 2012. A role for the centrosome and PAR-3 in the hand-off of MTOC function during epithelial polarization. *Curr. Biol.* 22:575–582. http://dx.doi.org/10.1016/j.cub.2012.02.044

Fernandez-Gonzalez, R., and J.A. Zallen. 2011. Oscillatory behaviors and hierarchical assembly of contractile structures in intercalating cells. *Phys. Biol.* 8:045005. http://dx.doi.org/10.1088/1478-3975/8/4/045005

Fletcher, G.C., E.P. Lucas, R. Brain, A. Tournier, and B.J. Thompson. 2012. Positive feedback and mutual antagonism combine to polarize Crumbs in the *Drosophila* follicle cell epithelium. *Curr. Biol.* 22:1116–1122. http://dx.doi.org/10.1016/j.cub.2012.04.020

Fu, X.D., and M. Ares Jr. 2014. Context-dependent control of alternative splicing by RNA-binding proteins. *Nat. Rev. Genet.* 15:689–701. http://dx.doi.org/10.1038/nrg3778

Graveley, B.R., A.N. Brooks, J.W. Carlson, M.O. Duff, J.M. Landolin, L. Yang, C.G. Artieri, M.J. van Baren, N. Boley, B.W. Booth, et al. 2011. The developmental transcriptome of *Drosophila melanogaster*. *Nature.* 471:473–479. http://dx.doi.org/10.1038/nature09715

Grawe, F., A. Wodarz, B. Lee, E. Knust, and H. Skaer. 1996. The *Drosophila* genes *crumbs* and *stardust* are involved in the biogenesis of adherens junctions. *Development.* 122:951–959.

Grosso, A.R., A.Q. Gomes, N.L. Barbosa-Morais, S. Caldeira, N.P. Thorne, G. Grech, M. von Lindern, and M. Carmo-Fonseca. 2008. Tissue-specific splicing factor gene expression signatures. *Nucleic Acids Res.* 36:4823–4832. http://dx.doi.org/10.1093/nar/gkn463

Hafezi, Y., J.A. Bosch, and I.K. Hariharan. 2012. Differences in levels of the transmembrane protein Crumbs can influence cell survival at clonal boundaries. *Dev. Biol.* 368:358–369. http://dx.doi.org/10.1016/j.ydbio.2012.06.001

Harris, T.J., and M. Peifer. 2005. The positioning and segregation of apical cues during epithelial polarity establishment in *Drosophila*. *J. Cell Biol.* 170:813–823. http://dx.doi.org/10.1083/jcb.200505127

Harris, T.J., and M. Peifer. 2007. aPKC controls microtubule organization to balance adherens junction symmetry and planar polarity during development. *Dev. Cell.* 12:727–738. http://dx.doi.org/10.1016/j.devcel.2007.02.011

Harris, T.J., and U. Tepass. 2010. Adherens junctions: from molecules to morphogenesis. *Nat. Rev. Mol. Cell Biol.* 11:502–514. http://dx.doi.org/10.1038/nrm2927

Hirai, T., and K. Chida. 2003. Protein kinase Cζ (PKCζ): activation mechanisms and cellular functions. *J. Biochem.* 133:1–7. http://dx.doi.org/10.1093/jb/mvg017

Inaba, M., Z.G. Venkei, and Y.M. Yamashita. 2015. The polarity protein Baz forms a platform for the centrosome orientation during asymmetric stem cell division in the *Drosophila* male germline. *eLife.* 4:04960. http://dx.doi.org/10.7554/eLife.04960

Jiang, T., R.F. McKinley, M.A. McGill, S. Angers, and T.J. Harris. 2015. A Par-1-Par-3-centrosome cell polarity pathway and its tuning for isotropic cell adhesion. *Curr. Biol.* 25:2701–2708. http://dx.doi.org/10.1016/j.cub.2015.08.063

Johnson, S.J., and R.N. Jackson. 2013. Ski2-like RNA helicase structures: common themes and complex assemblies. *RNA Biol.* 10:33–43. http://dx.doi.org/10.4161/rna.22101

Kalsotra, A., and T.A. Cooper. 2011. Functional consequences of developmentally regulated alternative splicing. *Nat. Rev. Genet.* 12:715–729. http://dx.doi.org/10.1038/nrg3052

Kelemen, O., P. Convertini, Z. Zhang, Y. Wen, M. Shen, M. Falaleeva, and S. Stamm. 2013. Function of alternative splicing. *Gene.* 514:1–30. http://dx.doi.org/10.1016/j.gene.2012.07.083

Kim, D.H., and J.J. Rossi. 1999. The first ATPase domain of the yeast 246-kDa protein is required for in vivo unwinding of the U4/U6 duplex. *RNA.* 5:959–971. http://dx.doi.org/10.1017/S135583829999012X

Kotak, S., C. Busso, and P. Gönczy. 2012. Cortical dynein is critical for proper spindle positioning in human cells. *J. Cell Biol.* 199:97–110. http://dx.doi.org/10.1083/jcb.201203166

Krahn, M.P., D. Egger-Adam, and A. Wodarz. 2009. PP2A antagonizes phosphorylation of Bazooka by PAR-1 to control apical-basal polarity in dividing embryonic neuroblasts. *Dev. Cell.* 16:901–908. http://dx.doi.org/10.1016/j.devcel.2009.04.011

Krahn, M.P., J. Bückers, L. Kastrup, and A. Wodarz. 2010. Formation of a Bazooka–Stardust complex is essential for plasma membrane polarity in epithelia. *J. Cell Biol.* 190:751–760. http://dx.doi.org/10.1083/jcb.201006029

Laggerbauer, B., T. Achsel, and R. Lührmann. 1998. The human U5-200kD DEXH-box protein unwinds U4/U6 RNA duplices *in vitro*. *Proc. Natl. Acad. Sci. USA.* 95:4188–4192. http://dx.doi.org/10.1073/pnas.95.8.4188

Lauber, J., P. Fabrizio, S. Teigelkamp, W.S. Lane, E. Hartmann, and R. Luhrmann. 1996. The HeLa 200 kDa U5 snRNP-specific protein and its homologue in *Saccharomyces cerevisiae* are members of the DEXH-box protein family of putative RNA helicases. *EMBO J.* 15:4001–4015.

Letizia, A., S. Ricardo, B. Moussian, N. Martín, and M. Llimargas. 2013. A functional role of the extracellular domain of Crumbs in cell architecture and apicobasal polarity. *J. Cell Sci.* 126:2157–2163. http://dx.doi.org/10.1242/jcs.122382

Liao, G., T. Nagasaki, and G.G. Gundersen. 1995. Low concentrations of nocodazole interfere with fibroblast locomotion without significantly affecting microtubule level: implications for the role of dynamic microtubules in cell locomotion. *J. Cell Sci.* 108:3473–3483.

Ligon, L.A., S. Karki, M. Tokito, and E.L. Holzbaur. 2001. Dynein binds to β-catenin and may tether microtubules at adherens junctions. *Nat. Cell Biol.* 3:913–917. http://dx.doi.org/10.1038/ncb1001-913

Lucas, E.P., and J.W. Raff. 2007. Maintaining the proper connection between the centrioles and the pericentriolar matrix requires *Drosophila* centrosomin. *J. Cell Biol.* 178:725–732. http://dx.doi.org/10.1083/jcb.200704081

Martinez-Campos, M., R. Basto, J. Baker, M. Kernan, and J.W. Raff. 2004. The *Drosophila* pericentrin-like protein is essential for cilia/flagella function, but appears to be dispensable for mitosis. *J. Cell Biol.* 165:673–683. http://dx.doi.org/10.1083/jcb.200402130

McGill, M.A., R.F. McKinley, and T.J. Harris. 2009. Independent cadherin-catenin and Bazooka clusters interact to assemble adherens junctions. *J. Cell Biol.* 185:787–796. http://dx.doi.org/10.1083/jcb.200812146

Mehalow, A.K., S. Kameya, R.S. Smith, N.L. Hawes, J.M. Denegre, J.A. Young, L. Bechtold, N.B. Haider, U. Tepass, J.R. Heckenlively, et al. 2003. CRB1 is essential for external limiting membrane integrity and photoreceptor morphogenesis in the mammalian retina. *Hum. Mol. Genet.* 12:2179–2189. http://dx.doi.org/10.1093/hmg/ddg232

Morais-de-Sá, E., V. Mirouse, and D. St Johnston. 2010. aPKC phosphorylation of Bazooka defines the apical/lateral border in *Drosophila* epithelial cells. *Cell.* 141:509–523. http://dx.doi.org/10.1016/j.cell.2010.02.040

Mozaffari-Jovin, S., T. Wandersleben, K.F. Santos, C.L. Will, R. Lührmann, and M.C. Wahl. 2013. Inhibition of RNA helicase Brr2 by the C-terminal tail of the spliceosomal protein Prp8. *Science.* 341:80–84. http://dx.doi.org/10.1126/science.1237515

Noble, S.M., and C. Guthrie. 1996. Identification of novel genes required for yeast pre-mRNA splicing by means of cold-sensitive mutations. *Genetics.* 143:67–80.

Otsu, N. 1979. A threshold selection method from gray-level histograms. *IEEE Trans. Syst. Man Cybern.* 9:62–66. http://dx.doi.org/10.1109/TSMC.1979.4310076

Park, J.W., K. Parisky, A.M. Celotto, R.A. Reenan, and B.R. Graveley. 2004. Identification of alternative splicing regulators by RNA interference in *Drosophila*. *Proc. Natl. Acad. Sci. USA.* 101:15974–15979. http://dx.doi.org/10.1073/pnas.0407004101

Parks, A.L., K.R. Cook, M. Belvin, N.A. Dompe, R. Fawcett, K. Huppert, L.R. Tan, C.G. Winter, K.P. Bogart, J.E. Deal, et al. 2004. Systematic generation of high-resolution deletion coverage of the *Drosophila melanogaster* genome. *Nat. Genet.* 36:288–292. http://dx.doi.org/10.1038/ng1312

Pellikka, M., G. Tanentzapf, M. Pinto, C. Smith, C.J. McGlade, D.F. Ready, and U. Tepass. 2002. Crumbs, the *Drosophila* homologue of human CRB1/RP12, is essential for photoreceptor morphogenesis. *Nature.* 416:143–149. http://dx.doi.org/10.1038/nature721

Pleiss, J.A., G.B. Whitworth, M. Bergkessel, and C. Guthrie. 2007. Transcript specificity in yeast pre-mRNA splicing revealed by mutations in core spliceosomal components. *PLoS Biol.* 5:e90. http://dx.doi.org/10.1371/journal.pbio.0050090

Pruitt, K.D., G.R. Brown, S.M. Hiatt, F. Thibaud-Nissen, A. Astashyn, O. Ermolaeva, C.M. Farrell, J. Hart, M.J. Landrum, K.M. McGarvey, et

al. 2014. RefSeq: an update on mammalian reference sequences. *Nucleic Acids Res.* 42:D756–D763. http://dx.doi.org/10.1093/nar/gkt1114

Raghunathan, P.L., and C. Guthrie. 1998. RNA unwinding in U4/U6 snRNPs requires ATP hydrolysis and the DEIH-box splicing factor Brr2. *Curr. Biol.* 8:847–855. http://dx.doi.org/10.1016/S0960-9822(07)00345-4

Rebay, I., R.J. Fleming, R.G. Fehon, L. Cherbas, P. Cherbas, and S. Artavanis-Tsakonas. 1991. Specific EGF repeats of Notch mediate interactions with Delta and Serrate: implications for Notch as a multifunctional receptor. *Cell.* 67:687–699. http://dx.doi.org/10.1016/0092-8674(91)90064-6

Riggleman, B., P. Schedl, and E. Wieschaus. 1990. Spatial expression of the *Drosophila* segment polarity gene armadillo is posttranscriptionally regulated by wingless. *Cell.* 63:549–560. http://dx.doi.org/10.1016/0092-8674(90)90451-J

Röper, K. 2012. Anisotropy of Crumbs and aPKC drives myosin cable assembly during tube formation. *Dev. Cell.* 23:939–953. http://dx.doi.org/10.1016/j.devcel.2012.09.013

Rösel, T.D., L.H. Hung, J. Medenbach, K. Donde, S. Starke, V. Benes, G. Rätsch, and A. Bindereif. 2011. RNA-Seq analysis in mutant zebrafish reveals role of U1C protein in alternative splicing regulation. *EMBO J.* 30:1965–1976. http://dx.doi.org/10.1038/emboj.2011.106

Santos, K.F., S.M. Jovin, G. Weber, V. Pena, R. Lührmann, and M.C. Wahl. 2012. Structural basis for functional cooperation between tandem helicase cassettes in Brr2-mediated remodeling of the spliceosome. *Proc. Natl. Acad. Sci. USA.* 109:17418–17423. http://dx.doi.org/10.1073/pnas.1208098109

Schmittgen, T.D., and K.J. Livak. 2008. Analyzing real-time PCR data by the comparative C(T) method. *Nat. Protoc.* 3:1101–1108. http://dx.doi.org/10.1038/nprot.2008.73

Schmoranzer, J., J.P. Fawcett, M. Segura, S. Tan, R.B. Vallee, T. Pawson, and G.G. Gundersen. 2009. Par3 and dynein associate to regulate local microtubule dynamics and centrosome orientation during migration. *Curr. Biol.* 19:1065–1074. http://dx.doi.org/10.1016/j.cub.2009.05.065

Schuldiner, O., D. Berdnik, J.M. Levy, J.S. Wu, D. Luginbuhl, A.C. Gontang, and L. Luo. 2008. *piggyBac*-based mosaic screen identifies a postmitotic function for cohesin in regulating developmental axon pruning. *Dev. Cell.* 14:227–238. http://dx.doi.org/10.1016/j.devcel.2007.11.001

Siegrist, S.E., and C.Q. Doe. 2007. Microtubule-induced cortical cell polarity. *Genes Dev.* 21:483–496. http://dx.doi.org/10.1101/gad.1511207

Simões, S.M., J.T. Blankenship, O. Weitz, D.L. Farrell, M. Tamada, R. Fernandez-Gonzalez, and J.A. Zallen. 2010. Rho-kinase directs Bazooka/Par-3 planar polarity during *Drosophila* axis elongation. *Dev. Cell.* 19:377–388. http://dx.doi.org/10.1016/j.devcel.2010.08.011

Spencer, W.C., G. Zeller, J.D. Watson, S.R. Henz, K.L. Watkins, R.D. McWhirter, S. Petersen, V.T. Sreedharan, C. Widmer, J. Jo, et al. 2011. A spatial and temporal map of *C. elegans* gene expression. *Genome Res.* 21:325–341. http://dx.doi.org/10.1101/gr.114595.110

Stearns, T., and M. Kirschner. 1994. In vitro reconstitution of centrosome assembly and function: the central role of γ-tubulin. *Cell.* 76:623–637. http://dx.doi.org/10.1016/0092-8674(94)90503-7

Tanentzapf, G., and U. Tepass. 2003. Interactions between the *crumbs*, *lethal giant larvae* and *bazooka* pathways in epithelial polarization. *Nat. Cell Biol.* 5:46–52. http://dx.doi.org/10.1038/ncb896

Tazi, J., N. Bakkour, and S. Stamm. 2009. Alternative splicing and disease. *Biochim. Biophys. Acta.* 1792:14–26. http://dx.doi.org/10.1016/j.bbadis.2008.09.017

Tepass, U. 1996. Crumbs, a component of the apical membrane, is required for zonula adherens formation in primary epithelia of *Drosophila*. *Dev. Biol.* 177:217–225. http://dx.doi.org/10.1006/dbio.1996.0157

Tepass, U. 2012. The apical polarity protein network in *Drosophila* epithelial cells: regulation of polarity, junctions, morphogenesis, cell growth, and survival. *Annu. Rev. Cell Dev. Biol.* 28:655–685. http://dx.doi.org/10.1146/annurev-cellbio-092910-154033

Tepass, U., and V. Hartenstein. 1994. The development of cellular junctions in the *Drosophila* embryo. *Dev. Biol.* 161:563–596. http://dx.doi.org/10.1006/dbio.1994.1054

Tepass, U., C. Theres, and E. Knust. 1990. *crumbs* encodes an EGF-like protein expressed on apical membranes of *Drosophila* epithelial cells and required for organization of epithelia. *Cell.* 61:787–799. http://dx.doi.org/10.1016/0092-8674(90)90189-L

Thibault, S.T., M.A. Singer, W.Y. Miyazaki, B. Milash, N.A. Dompe, C.M. Singh, R. Buchholz, M. Demsky, R. Fawcett, H.L. Francis-Lang, et al. 2004. A complementary transposon tool kit for *Drosophila melanogaster* using P and piggyBac. *Nat. Genet.* 36:283–287. http://dx.doi.org/10.1038/ng1314

Thompson, B.J., F. Pichaud, and K. Röper. 2013. Sticking together the Crumbs – an unexpected function for an old friend. *Nat. Rev. Mol. Cell Biol.* 14:307–314. http://dx.doi.org/10.1038/nrm3568

Trapnell, C., D.G. Hendrickson, M. Sauvageau, L. Goff, J.L. Rinn, and L. Pachter. 2013. Differential analysis of gene regulation at transcript resolution with RNA-seq. *Nat. Biotechnol.* 31:46–53. http://dx.doi.org/10.1038/nbt.2450

Truong Quang, B.A., M. Mani, O. Markova, T. Lecuit, and P.F. Lenne. 2013. Principles of E-cadherin supramolecular organization *in vivo*. *Curr. Biol.* 23:2197–2207. http://dx.doi.org/10.1016/j.cub.2013.09.015

Venken, K.J., J.W. Carlson, K.L. Schulze, H. Pan, Y. He, R. Spokony, K.H. Wan, M. Koriabine, P.J. de Jong, K.P. White, et al. 2009. Versatile P[acman] BAC libraries for transgenesis studies in *Drosophila melanogaster*. *Nat. Methods.* 6:431–434. http://dx.doi.org/10.1038/nmeth.1331

Walther, R.F., and F. Pichaud. 2010. Crumbs/DaPKC-dependent apical exclusion of Bazooka promotes photoreceptor polarity remodeling. *Curr. Biol.* 20:1065–1074. http://dx.doi.org/10.1016/j.cub.2010.04.049

Wang, E.T., R. Sandberg, S. Luo, I. Khrebtukova, L. Zhang, C. Mayr, S.F. Kingsmore, G.P. Schroth, and C.B. Burge. 2008. Alternative isoform regulation in human tissue transcriptomes. *Nature.* 456:470–476. http://dx.doi.org/10.1038/nature07509

Wang, Y.C., Z. Khan, M. Kaschube, and E.F. Wieschaus. 2012. Differential positioning of adherens junctions is associated with initiation of epithelial folding. *Nature.* 484:390–393. http://dx.doi.org/10.1038/nature10938

Warn, R.M., and A. Warn. 1986. Microtubule arrays present during the syncytial and cellular blastoderm stages of the early *Drosophila* embryo. *Exp. Cell Res.* 163:201–210. http://dx.doi.org/10.1016/0014-4827(86)90573-2

Wickramasinghe, V.O., M. Gonzàlez-Porta, D. Perera, A.R. Bartolozzi, C.R. Sibley, M. Hallegger, J. Ule, J.C. Marioni, and A.R. Venkitaraman. 2015. Regulation of constitutive and alternative mRNA splicing across the human transcriptome by PRPF8 is determined by 5′ splice site strength. *Genome Biol.* 16:201. http://dx.doi.org/10.1186/s13059-015-0749-3

Wirtz-Peitz, F., and J.A. Zallen. 2009. Junctional trafficking and epithelial morphogenesis. *Curr. Opin. Genet. Dev.* 19:350–356. http://dx.doi.org/10.1016/j.gde.2009.04.011

Wodarz, A., U. Hinz, M. Engelbert, and E. Knust. 1995. Expression of crumbs confers apical character on plasma membrane domains of ectodermal epithelia of *Drosophila*. *Cell.* 82:67–76. http://dx.doi.org/10.1016/0092-8674(95)90053-5

Xu, D., S. Nouraini, D. Field, S.-J. Tang, and J.D. Friesen. 1996. An RNA-dependent ATPase associated with U2/U6 snRNAs in pre-mRNA splicing. *Nature.* 381:709–713. http://dx.doi.org/10.1038/381709a0

Yap, A.S., G.A. Gomez, and R.G. Parton. 2015. Adherens junctions revisualized: Organizing cadherins as nanoassemblies. *Dev. Cell.* 35:12–20. http://dx.doi.org/10.1016/j.devcel.2015.09.012

Zallen, J.A., and E. Wieschaus. 2004. Patterned gene expression directs bipolar planar polarity in *Drosophila*. *Dev. Cell.* 6:343–355. http://dx.doi.org/10.1016/S1534-5807(04)00060-7

Zhang, L., T. Xu, C. Maeder, L.O. Bud, J. Shanks, J. Nix, C. Guthrie, J.A. Pleiss, and R. Zhao. 2009. Structural evidence for consecutive Hel308-like modules in the spliceosomal ATPase Brr2. *Nat. Struct. Mol. Biol.* 16:731–739. http://dx.doi.org/10.1038/nsmb.1625

Zhao, C., D.L. Bellur, S. Lu, F. Zhao, M.A. Grassi, S.J. Bowne, L.S. Sullivan, S.P. Daiger, L.J. Chen, C.P. Pang, et al. 2009. Autosomal-dominant retinitis pigmentosa caused by a mutation in SNRNP200, a gene required for unwinding of U4/U6 snRNAs. *Am. J. Hum. Genet.* 85:617–627. http://dx.doi.org/10.1016/j.ajhg.2009.09.020

Zou, J., X. Wang, and X. Wei. 2012. Crb apical polarity proteins maintain zebrafish retinal cone mosaics via intercellular binding of their extracellular domains. *Dev. Cell.* 22:1261–1274. http://dx.doi.org/10.1016/j.devcel.2012.03.007